2010

A Spirocyclohexyl Nitroxide Amino Acid Spin Label for Pulsed EPR Distance Measurements

Andrzej Rajca
University of Nebraska - Lincoln, arajca1@unl.edu

Velavan Kathirvelu
University of Denver

Sandip K. Riy
University of Nebraska-Lincoln

Maren Pink
Indiana University

Suchada Rajca
University of Nebraska-Lincoln, srajca1@unl.edu

See next page for additional authors

PMCID: PMC3103209

Published in final edited form as:
Chemistry. 2010 May 17; 16(19): 5778–5782. doi:10.1002/chem.200903102.

A Spirocyclohexyl Nitroxide Amino Acid Spin Label for Pulsed EPR Distance Measurements

Prof. Andrzej Rajca[*,[a]], **Dr. Velavan Kathirvelu**[[b]], **Dr. Sandip K. Roy**[[a]], **Dr. Maren Pink**[[c]], **Dr. Suchada Rajca**[[a]], **Mr. Santanu Sarkar**[[a]], **Prof. Sandra S. Eaton**[[b]], and **Prof. Gareth R. Eaton**[*,[b]]

[a]Department of Chemistry University of Nebraska Lincoln, NE 68588-0304

[b]Department of Chemistry and Biochemistry University of Denver Denver, CO 80208-2436

[c]Department of Chemistry Indiana University Bloomington, IN 47405-7102

Abstract

Site-directed spin labeling (SDSL) and electron paramagnetic resonance (EPR) spectroscopy offer accurate, sensitive tools for the characterization of structure and function of macromolecules and their assemblies. A new rigid spin label, spirocyclohexyl nitroxide α-amino acid and its *N*-(9-fluorenylmethoxycarbonyl) (Fmoc) derivative, has been synthesized that exhibit slow enough spin echo dephasing to permit accurate distance measurements by pulse EPR at temperatures up to 125 K in 1:1 water:glycerol and at higher temperatures in matrices with higher glass transition temperatures. Distance measurements in the liquid nitrogen temperature range are less expensive than those that require liquid helium, which will greatly facilitate applications of pulsed EPR to the study of structure and conformation for peptides and proteins.

Keywords

spin labels; EPR; radicals; spiro compounds; spin relaxation

Introduction

Accurate and sensitive methods to probe structure and function of proteins, nucleic acids, and their assemblies are important for understanding disease processes and interventions, and contribute to drug design. Conformations and interactions of these macromolecules can be probed using nuclear magnetic resonance (NMR), electron paramagnetic resonance (EPR), fluorescence spectroscopy, and small angle scattering (SAS).

An exciting and important development is site-directed spin labeling (SDSL) of biomacromolecules, mostly proteins, but recently also RNA and DNA, and the use of pulsed EPR spectroscopy to measure distances between labels separated by 2–8 nm.[1–11] The spin-labeling/pulsed EPR technique is one of the best methods for accurate measurement of conformational changes and characterization of flexible regions of biomacromolecules, with minimum perturbation by relatively small labels. Applications are however impeded by the electron spin-spin relaxation properties of spin labels. In contrast to advances in SDSL and pulsed EPR techniques, improvements in spin labels have lagged behind.

[*] arajca1@unl.edu . [*] gareth.eaton@du.edu .

Supporting information for this article is available on the WWW under http://www.chemeurj.org/ or from the author.

Double electron resonance (DEER) and double quantum coherence (DQC) methods for interspin distance determination are based upon detection of an electron spin echo. The time constant for decay of the echo as a function of the time between pulses is the phase memory time T_m. The longer T_m, the longer the distance one can measure, and the more precisely the distribution of distances can be defined.[10, 12] Most spin labels, including the widely used 1-oxyl-2,2,5,5-tetramethyl-3-pyrroline-3-(methyl)methanethiosulfonate (MTSSL) (Figure 1), are nitroxide radicals in which the N-O radical moiety is sterically shielded by two gem-dimethyl-substituted quaternary carbons to provide kinetic stability. At temperatures above about 70 K rotation of these methyl groups averages inequivalent couplings of the unpaired electron to the protons on the EPR timescale, which decreases T_m,[13–15] and imposes a 50–65 K upper limit on the temperature at which distance measurements can be made with optimum performance.[12] To achieve these temperatures liquid helium is required. The gemdimethyl structure motif in spin labels has remained unchanged since McConnell's pioneering studies.[16] Recently, Velavan et al. showed that nitroxides such as 7-aza-4,12,15-trihydroxydispiro[5.1.5.3]hexadecane-7-oxyl (trihydroxy-DICPO) (Figure 1), which are stabilized by spirocyclohexyl groups at the 2-and 6-positions of the piperidine ring exhibit values of T_m in 1:1 water:glycerol that are long enough for pulsed EPR distance measurements up to about 125 K.[17] New spin labels with cyclohexyl groups instead of gem-dimethyls would make it possible to perform distance measurements with less expensive liquid nitrogen.

In spin labels such as MTSSL, the linkage between the protein and the nitroxide N-O group is relatively flexible and the distance between the protein backbone and the N-O moiety is about 0.7 nm. Another spin label is 2,2,6,6-tetramethylpiperidine-1-oxyl-4-amino-4-carboxylic acid (TOAC) (Figure 1) – first synthesized by Rassat and Rey.[18] This unnatural α-amino acid greatly improves EPR distance measurements because it can be rigidly built into a polypeptide chain, though it poses more strict restraints on backbone geometry than natural amino acids. Although incorporation of TOAC into peptides and proteins is more difficult compared to MTSSL, TOAC has been used to study protein folding, backbone dynamics, and peptide aggregation.[8, 19–29]

Here we report the synthesis and characterization of spirocyclohexyl nitroxide α-amino acid **1** (7-aza-dispiro[5.1.5.3]hexadecane-7-oxyl-15-amino-15-carboxylic acid and its *N*-(9-fluorenylmethoxycarbonyl) (Fmoc) derivative, Fmoc-**1**, for incorporation into a peptide via solid-phase synthesis, analogous to that for TOAC (Figure 1).[33] The bulky spirocyclohexyl groups may make incorporation of **1** into a peptide more challenging than of TOAC. These bulky groups may also pose greater constraints on conformations of the peptide backbone, as well as on packing of the side groups, however, the significance of these constraints is likely to depend on the peptide. To distinguish between the impact of intramolecular motions and molecular librations,[13, 30, 31] the temperature dependence of T_m for **1** in 1:1 water:glycerol is compared with that in a poly(vinyl alcohol)–borate glass (PVA/borate)[32] that has a glass transition temperature well above ambient. This new spin label has long enough T_m at 125 K to perform DEER with liquid nitrogen in 1:1 water:glycerol, and at higher temperatures in PVA/borate.

Results and Discussion

Synthesis

The synthesis of nitroxide α-amino acid **1** and its Fmoc-protection is outlined in Scheme 1. Nitroxide **2** was prepared by the modified method of Bobbit and coworkers,[34] and then converted to hydantoin nitroxide **3** in high yield. Using the method for preparation of TOAC,[18] direct hydrolysis of hydantoin nitroxide **3** under forcing conditions, provided α-amino acid nitroxide **1** in about 50% yield. However, it was difficult to isolate **1** with 100%

spin purity and free from the intermediate hydrolysis product (hydantoic acid).[35] The increased steric shielding of the 15-position by the spirocyclohexane rings of **1**, compared to the methyl groups of TOAC, may contribute to the incomplete conversion of the intermediate hydantoic acid to **1**. The synthesis was modified by following Rebek's method for conversion of hydantoin-nucleosides to the corresponding amino acid-nucleosides,[36] in two steps. Therefore, hydantoin nitroxide **3** was converted to the di-Boc derivative **4**, followed by hydrolysis under relatively mild conditions to provide **1** in the zwitterionic form, as precipitate from water.

The use of an amino acid as spin label is best implemented using Fmoc as an *N*-protecting group, to enable incorporation of the spin label in the peptide chain via solid-phase synthesis.[37, 38] Therefore, **1** was *N*-protected to provide Fmoc-**1** in ~50% yield and ~100% spin purity (Scheme 1).

Spectroscopic data for **1** and Fmoc-**1** are similar to those reported for their TOAC analogues (Supporting Information).[37, 38] In particular, ^{1}H NMR spectrum for a 0.18 M lithium salt of **1** in D_2O shows a broad resonance with a shoulder at about −1 ppm, compared to the single resonance at −5.7 ppm reported for a saturated solution of TOAC in D_2O at pH 12.[39] Also, ^{1}H NMR spectra for **1** and Fmoc-**1** indicate that these nitroxide radicals possess high spin purity (Figures S17 and S18, Supporting Information).

X-ray crystallography

Although a single crystals of **1** could not be grown, the structure and conformation of hydantoin nitroxide **3** was determined by X-ray crystallography using synchrotron radiation (Figure 2).[40] Two different crystal structures were observed, designated as structure A and B, and one of them is the solvent polymorph of the other. Both structures have space group P-1 with two unique molecules (molecule A and B) per asymmetric unit; the asymmetric unit of structure B includes half of a solvent molecule (ethyl acetate). The two structures differ in the connectivity of hydrogen bonds between hydantoin moieties (Figures S4 and S5, Supporting Information).

In both structures A and B, the piperidine ring of molecule A adopts a twist-boat conformation and that of molecule B adopts a chair conformation with an approximately C_s symmetry (Figure 2). In both unique molecules with chair conformations, the carbonyl group of the hydantoin is in the “equatorial” position. The spirocyclic cyclohexane rings of all unique molecules are in chair conformations, in which the nitroxide moiety is in an equatorial position. In peptides, the TOAC piperidine ring adopts a twist-boat conformation.[41, 42]

The co-existence of unique molecules with twist-boat and chair piperidine rings in single crystals of **3** suggests that the energy difference between the two conformations is small. This energy difference was calculated using the B3LYP density functional method with the triple-ζ basis set 6–311+G(d,p).[43] Optimization of the structures starting from the X-ray determined geometries for molecule A and molecule B in structure A gives a preference for chair over twist-boat by 0.9 kcal mol^{-1} (corrected for zero-point energies).[44]

Spin Echo Dephasing

The dephasing rates, $1/T_m$ (Figure 3), for **1** in 1:1 water:glycerol are similar to those for trihydroxy-DICPO,[17] but they are very different from methyl-containing MTSSL which is commonly used for DEER experiments, for which rotation of the gem-dimethyls dominates dephasing between about 80 and 250 K.[45] The relatively slow dephasing rates for **1** up to about 125 K will make it possible to perform DEER experiments in this liquid-nitrogen accessible temperature range. In 1:1 water:glycerol which has a glass transition temperature

about 175 K,[46, 47] the dephasing rates for both MTSSL and **1** increase rapidly above about 125 K (Figure 3), which is attributed to increasing molecular motion as the glass softens.

The dramatic impact of the changes in $1/T_m$ from MTSSL to **1** on the spin echo intensity at the interpulse spacings (τ) of 1 to 2 μs that are commonly used for DEER and DQC experiments is evident from the plots shown in Figure 4. The echo intensity at the τ values used for the DEER or DQC experiments determines the signal-to-noise. Longer T_m provides adequate signal-to-noise at longer τ values, which permits measurement of longer interspin distances and more accurate definition of distributions of interspin distances.

To determine whether piperidine ring dynamics impact spin echo dephasing at higher temperatures, echo decays were studied in PVA/borate, which has a glass transition temperature well above ambient. In this glass, $1/T_m$ for spirocyclic nitroxides **1** and trihydroxy-DICPO, which have 6-membered piperidine rings, exhibits negligible temperature dependence up to 125 K, then increases gradually with increasing temperature up to 350 K (Figure 5). In contrast, methyl rotation dominates echo dephasing between about 80 and 250 K for both MTSSL which has a 5-membered pyrroline ring and for 1-oxyl-2,2,6,6-tetramethyl-4-hydroxypiperidine (Tempol), which has a 6-membered piperidine ring. For MTSSL and Tempol the temperature dependence of $1/T_m$ above 300 K is similar to that for **1** and for trihydroxy-DICPO. At 350 K T_m for trihydroxy-DICPO and for **1** are 200 ns and 70 ns longer, respectively, than T_m for MTSSL or Tempol.

Conclusion

The synthesis of **1** demonstrates that it is possible to prepare a spin label with a short rigid linker analogous to that of TOAC and the favorable electron spin relaxation properties of spirocyclohexyl nitroxides. The shorter distance between the α-carbon and the paramagnetic center for **1** than for MTSSL will decrease the range of conformations present in spin-labeled samples. The negligible temperature dependence of $1/T_m$ for **1** in 1:1 water:glycerol facilitates EPR distance measurements up to 125 K with liquid nitrogen. The spin lattice relaxation rates ($1/T_1$) for **1** at 125 K are about 4 times faster than for MTSSL at 65 K (Figure S2, Supporting Information). The differences in Boltzmann populations, which determine echo intensity, decrease approximately linearly with increasing temperature. The loss in signal intensity due to the decrease in the difference in populations of the spin states on increasing temperature from 65 K to about 125 K is approximately compensated by the faster pulse repetition rates that can be used at 125 K. Thus, incorporation of **1** into peptides and proteins should permit EPR distance measurements using liquid nitrogen at temperatures up to about 125 K with sensitivity similar to that which has previously been possible only by using liquid helium.

Spin echo dephasing experiments as a function of temperature in rigid PVA/borate demonstrate that the faster dephasing rate for MTSSL and **1** above about 150 K in 1:1 water:glycerol is due to the onset of motion as the glass softens. MTSSL and Tempol have different ring structures, but have similar $1/T_m$ rates in PVA/borate above room temperature, and $1/T_m$ of **1** is similar to that for MTSSL at 350 K, which suggests that piperidine ring dynamics do not dominate dephasing at temperatures up to 350 K. These results demonstrate that the use of rigid matrices with high glass transition temperatures should permit pulsed EPR distance measurements with **1** as a spin label at temperature well above 125 K. Slower dephasing for trihydroxy-DICPO than for **1** above about 200 K could be attributed to hydrogen-bonding between the three hydroxyl groups and the PVA/borate matrix, which would decrease librational motion.[13, 31] The dependence of T_m on motion above about 200 K suggests that when **1** is incorporated into a peptide, T_m may increase.

Experimental Section

Experimental details on the synthesis and characterization of amino acid nitroxide and its Fmoc-derivative, Fmoc-**1**, as well as description of pulsed EPR experiments, may be found in the Supporting Information.

Supplementary Material

Refer to Web version on PubMed Central for supplementary material.

Acknowledgments

This research was supported by NSF CHE-0718117 (Nebraska), NIH NIBIB EB008484 (Nebraska), Nebraska Research Initiative, and NIH NIBIB EB002807 (Denver). Use of the APS for crystallography is supported by the U. S. DOE, Office of Science, Office of Basic Energy Sciences, Contract No. DE-AC02-06CH11357 and ChemMatCARS by the National Science Foundation/DOE grant, CHE-0535644. We thank Professor David Thomas (Minnesota) for discussions and Dr. Shuzhang Xiao (Nebraska) for attempts to optimize direct hydrolysis of hydantoin to amino acid.

References

[1]. Dzuba SA. Russian Chem. Rev. 2007; 76:699–713.

[2]. Berliner, LJ.; Eaton, GR.; Eaton, SS., editors. Distance Measurements in Biological Systems by EPR. Kluwer; New York: 2000.

[3]. Eaton GR, Eaton SS. Specialist Periodical Report on Electron Spin Resonance. 2008; 21:59–75.

[4]. Jeschke G. ChemPhysChem. 2002; 3:927–932. [PubMed: 12503132]

[4]. Jeschke G. Curr. Opin. Solid State Mat. Sci. 2003; 7:181–188.

[6]. Jeschke G, Chechik V, Ionita P, Godt A, Zimmermann H, Banham J, Timmel CR, Hilger D, Jung H. Appl. Magn. Reson. 2006; 30:473–498.

[7]. Klug CS, Feix JB. Biol. Magn. Reson. 2005; 24:269–308.

[8]. McNulty J, Silapie JL, Carnevali M, Farrar TC, Griffin RG, Formaggio F, Crisma M, Toniolo C, Millhauser G. Biopolymers. 2000; 55:479–485. [PubMed: 11304675]

[9]. Schiemann O, Piton N, Plackmeyer J, Bode BE, Prisner TF, Engels JW. Nature Protocols. 2007; 2:904–923.

[10]. Borbat PP, Davis JH, Butcher SE, Freed JH. J. Am. Chem. Soc. 2004; 126:7746–7747. [PubMed: 15212500]

[11]. Lovett JE, Hoffmann M, Cnossen A, Shutter ATJ, Hogben HJ, Warren JE, Pascu SI, Kay CWM, Timmel CR, Anderson HL. J. Am. Chem. Soc. 2009; 131:13852–13859. [PubMed: 19736940]

[12]. Jeschke G, Polyhach Y. Phys. Chem. Chem. Phys. 2007; 9:1895–1910. [PubMed: 17431518]

[13]. Dzuba SA, Maryasov AG, Salikhov AK, Tsvetkov YD. J. Magn. Reson. 1984; 58:95–117.

[14]. Nakagawa K, Candelaria MB, Chik WWC, Eaton SS, Eaton GR. J. Magn. Reson. 1992; 98:81–91.

[15]. Lindgren M, Eaton GR, Eaton SS, Jonsson B-H, Hammarstrom P, Svensson M, Carlsson U. J. Chem. Soc., Perkin Trans. 1997; 2:2549–2554.

[16]. Stone TJ, Buckman T, Nordio PL, McConnell HM. Proc. Nat. Acad. Sci. USA. 1965; 54:1010–1017. [PubMed: 5219813]

[17]. Kathirvelu V, Smith C, Parks C, Mannan MA, Miura Y, Takeshita K, Eaton SS, Eaton GR. Chem. Commun. 2009:454–456.

[18]. Rassat A, Rey P. Bull. Chim. Soc. Fr. 1967:815–817.

[19]. Hanson P, Martinez G, Millhauser G, Formaggio F, Crisma M, Toniolo C, Vita C. J. Am. Chem. Soc. 1996; 118:271–272.

[20]. Toniolo C, Crisma M, Formaggio F. Biopolymers. 1998; 47:153–158.

[21]. Karim CB, Kirby TL, Zhang Z, Nesmelov Y, Thomas DD. Proc. Nat. Acad. Sci. USA. 2004; 101:14437–14442. [PubMed: 15448204]

[22]. Zamoon J, Nitu F, Karim C, Thomas DD, Veglia G. Proc. Nat. Acad. Sci. USA. 2005; 102:4747–4752. [PubMed: 15781867]

[23]. Karim CB, Zhang Z, Howard EC, Torgersen KD, Thomas DD. J. Mol. Biol. 2006; 358:1032–1040. [PubMed: 16574147]

[24]. Zhang Z, Thomas DD, Karim CB. Nature Protocols. 2006; 2:43–49.

[25]. Zhang Z, Remmer HA, Thomas DD, Karim CB. Biopolymers. 2007; 88:29–35. [PubMed: 17066471]

[26]. Nesmelov YE, Karim CB, Song L, Fajer P, Thomas DD. Biophys. J. 2007; 93:2805–2812. [PubMed: 17573437]

[27]. Marsh D, Toniolo C. J. Magn. Reson. 2008; 190:211–221. [PubMed: 18042415]

[28]. Bartucci R, Guzzi R, DeZotti M, Toniolo C, Sportelli L, Marsh D. Biophys. J. 2008; 94:2698–2705. [PubMed: 18096632]

[29]. Milov AD, Samoilova RI, Tsvetkov YD, DeZotti M, Toniolo C, Raap J. J. Phys. Chem. B. 2008; 112:13469–13472. [PubMed: 18837536]

[30]. Dzuba SA. Physics Lett. A. 1996; 213:77–84.

[31]. Paschenko SV, Toropov YV, Dzuba SA, Tsvetkov YD, Vorobiev AK. J. Chem. Phys. 1999; 110:8150–8154.

[32]. Nijenhuis KT. Polym. Bull. 2007; 58:27–42.

[33]. Karim CB, Zhang Z, Thomas DD. Nature Protocols. 2007; 2:42–49.

[34]. Ma Z, Huang Q, Bobbitt JM. J. Org. Chem. 1993; 58:4837–4843.

[35]. Ware E. Chem. Rev. 1950; 46:403–470.

[36]. Kubik S, Meissner RS, Rebek J Jr. Tetrahedron Lett. 1994; 35:6635–6638.

[37]. Marchetto R, Schreier S, Nakaie CR. J. Am. Chem. Soc. 1993; 115:11041–11043.

[38]. Smythe ML, Nakaie CR, Marshall GR. J. Am. Chem. Soc. 1995; 117:10555–10562.

[39]. Rastrelli F, Bagno A. Chem. Eur. J. 2009; 15:7990–8004.

[40]. Coordinates and other crystallographic information for polymorphs A and B of nitroxide **3** have been deposited with the Cambridge Crystallographic Database Center with deposition numbers CCDC 741375 and 741376, respectively.

[41]. Flippen-Anderson JL, George C, Valle G, Valente E, Bianco A, Formaggio F, Crisma M, Toniolo C. Int. J. Pept. Prot. Res. 1996; 47:231–238.

[42]. Crisma M, Deschamps JR, George C, Flippen-Anderson JL, Kaptein B, Broxterman QB, Moretto A, Oancea S, Jost M, Formaggio F, Toniolo C. J. Peptide Res. 2005; 65:564–579. [PubMed: 15885116]

[43]. Frisch, MJ., et al. Gaussian, Inc.; Wallingford, CT: 2004.

[44]. The preference for the chair conformation is only 0.4 kcal mol^{-1} at the X-ray determined geometries (Table S8, Supporting Information).

[45]. Zecevic A, Eaton GR, Eaton SS, Lindgren M. Mol. Phys. 1998; 95:1255–1263.

[46]. Blochowicz T, Kudik A, Benkhof S, Senker J, Rossler E, Hinze G. J. Chem. Phys. 1999; 110:12011–12022.

[47]. Murphy SSN. J. Phys. Chem. B. 2000; 104:6955–6962.

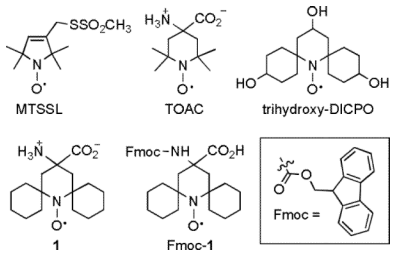

Figure 1.
Nitroxide spin labels and related radicals.

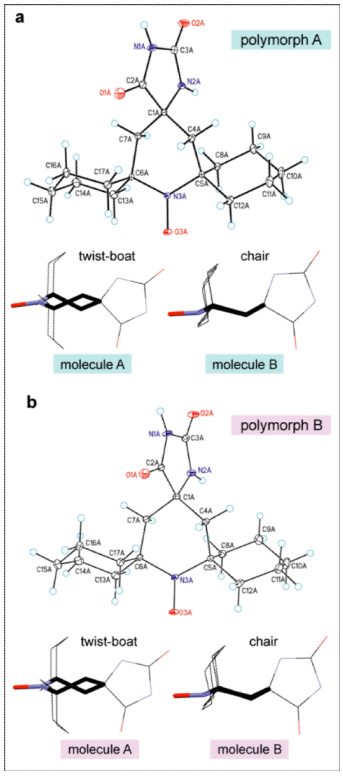

Figure 2.

Molecular structure and conformation for hydantoin nitroxide **3**. (**a**) Structure A. (**b**) Structure B. ORTEP plots with thermal ellipsoids set at 50% probability show one of the two unique molecules, without solvent of crystallization.

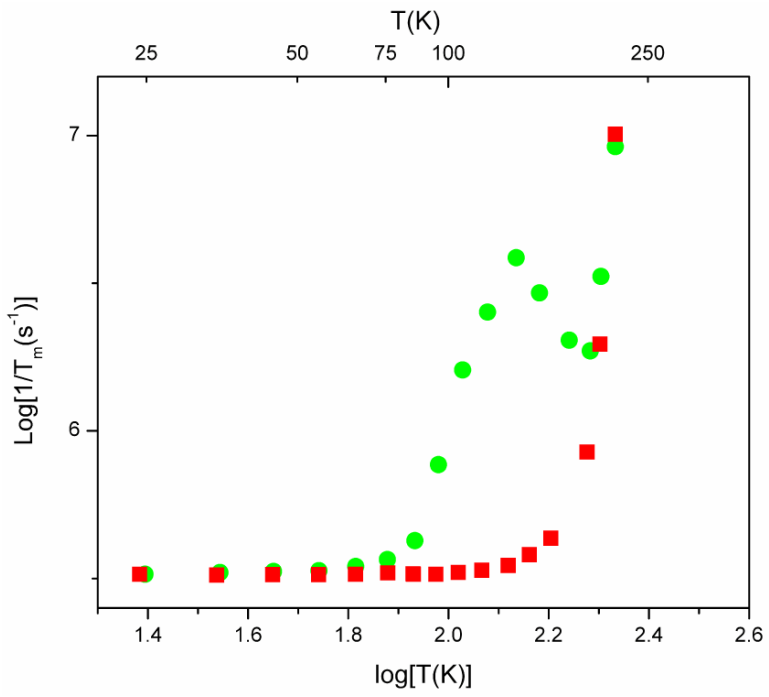

Figure 3.
Temperature dependence of spin echo dephasing rates, $1/T_m$, in 1:1 water:glycerol for **1** (■), and MTSSL (●).

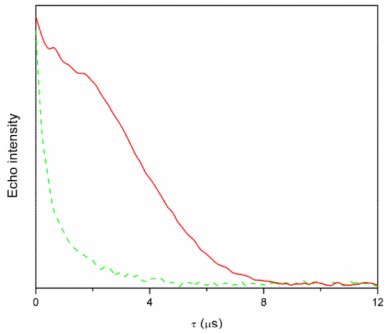

Figure 4.
Intensity of spin echo in 1:1 water:glycerol at 105 K as a function of the time between pulses (τ) for **1** (solid red line), and MTSSL (dashed green line).

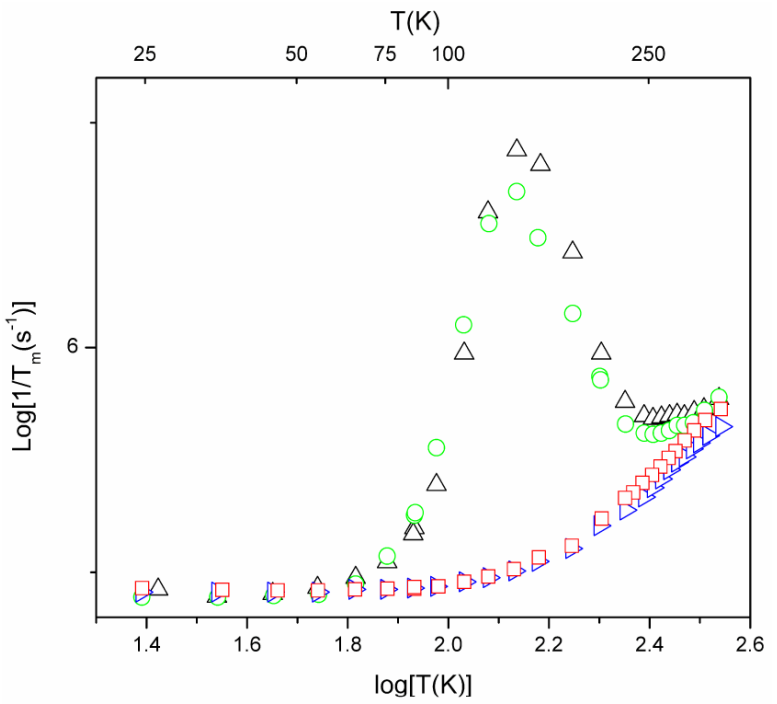

Figure 5.
Temperature dependence of spin echo dephasing rates, $1/T_m$, in 1:1 PVA/borate for **1** (□), trihydroxy-DICPO (▷), Tempol (Δ), and MTSSL (O)

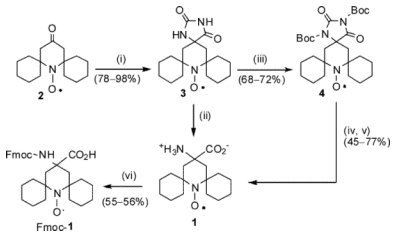

Scheme 1.

Synthesis of spirocyclic nitroxide α-amino acid **1** and its *N*-protected derivative Fmoc-**1**. (i) $(NH_4)_2CO_3$, NaCN, H_2O, 75 °C, 35 h; (ii) $Ba(OH)_2$, H_2O, then $(NH_4)_2CO_3$, H_2O, 140–170 °C; (iii) Boc_2O, DMAP, THF, 25 °C, 3 h; (iv) LiOH, 40–45 °C, 12 h; (v) HCl, 0 °C, pH 6.5; (vi) Fmoc-succinimidyl carbonate (Fmoc-OSu), triethylamine, acetonitrile/water, pH 8–9, 25 °C, 45 min, then 20% aqueous citric acid, 0 °C, 15 min

CHEMISTRY
A EUROPEAN JOURNAL

Supporting Information

A Spirocyclohexyl Nitroxide Amino Acid Spin Label for Pulsed EPR Spectroscopy Distance Measurements

Andrzej Rajca,*[a] Velavan Kathirvelu,[b] Sandip K. Roy,[a] Maren Pink,[c] Suchada Rajca,[a] Santanu Sarkar,[a] Sandra S. Eaton,[b] and Gareth R. Eaton*[b]

chem_200903102_sm_miscellaneous_information.pdf

Supporting Information

A Spirocyclohexyl Nitroxide Amino Acid Spin Label for Pulsed EPR Distance Measurements

Andrzej Rajca[*1], *Velavan Kathirvelu*[2], *Sandip K. Roy*[1], *Maren Pink*[3], *Suchada Rajca*[1], *Santanu Sarkar*[1], *Sandra S. Eaton*[2], *Gareth R. Eaton*[*2]

[1]Department of Chemistry, University of Nebraska, Lincoln, NE 68588-0304. [2]Department of Chemistry and Biochemistry, University of Denver, Denver, CO 80208-2436. [3]Department of Chemistry, Indiana University, Bloomington, IN 47405-7102

Table of Contents

1. EPR spectroscopy.

Samples in poly(vinyl alcohol)–borate glasses (PVA/borate). Poly(vinyl alcohol) (0.4 g, Sigma-Aldrich, MW 13,000–23,000, 98% hydrolyzed) and boric acid (0.18 g, Mallinckrodt, Analytical grade) were dissolved in a minimum amount of water individually and the solution of boric acid was diluted with methanol to about 20 mL. The hot solutions were mixed immediately. The radicals were dissolved in methanol and added to the poly(vinyl alcohol) : boric acid mixture. A thin layer of the mixture was dried overnight at 50 °C to make a film of PVA/borate. The glasses were ground to a fine powder, transferred to a 4 mm OD quartz EPR tube, and dried for a week at 55 °C under vacuum (10–20 mTorr), followed by flame sealing of the tube. The radical concentrations in the dried samples were 0.1 to 0.5 mM.

CW EPR spectra. X-band CW spectra were recorded on a Varian E9 or a Bruker E580 at the University of Denver or a Bruker EMX at Nebraska. DPPH (g = 2.0036) was used as the g-value standard.

Pulsed EPR. Spin-lattice relaxation rates ($1/T_1$) were measured on a locally-constructed X-band saturation recovery (SR) spectrometer.[2] Below 150 K a rectangular resonator with Q ~ 3000 was used. Above 150 K a loop-gap resonator with Q ~ 1000, and therefore lower deadtime, was used. Relaxation rates as a function of temperature between 100 and 295 K were measured at the magnetic field position that corresponds to the maximum intensity in the absorption spectrum. Artifacts due to switching and cavity heating were removed by subtraction of an off-resonance signal. To minimize the impact of

spectral diffusion, the pump pulse length was longer than T_1. Single exponentials gave good fits to the saturation recovery curves.

Electron spin echo (ESE) experiments were performed on a Bruker E580 spectrometer using an over-coupled split ring resonator in an Oxford CF 935 cryostat or on a locally-constructed X-band ESE spectrometer with a locally-modified rectangular resonator.[3] The Q of the over-coupled resonator was about 150. The field dependence of T_1 at 85 K was measured by inversion recovery with a π-τ_{var}-$\pi/2$-τ-π-τ-echo pulse sequence, τ = 370 ns and initial τ_{var} = 120 ns. The pulse power was adjusted to maximize the two-pulse echo intensity. The echo dephasing times (T_m) were measured with a $\pi/2$-τ-π-τ-echo pulse sequence, 20 and 40 ns pulse lengths, and initial τ = 120 ns. For both the T_1 and T_m measurements, the data acquisition window was about ten times the relaxation time. Uncertainties in values of T_1 and T_m are about 5%.

Calculation of T_m. Echo decay curves were analyzing by fitting with the equation: $y = y_0 exp\left(-\left(\frac{x}{T_m}\right)^n\right) + c$. At low temperatures the limiting values of n are about 2 at 25 K. Values of n > 1 are attributed to dephasing via nuclear spin diffusion of solvent protons, as is typical for nitroxides at low temperature.[4, 5] In temperature regions where dynamic processes impact dephasing, n decreases to about 1. To facilitate comparisons of trends over the full range of temperatures studied, n = 1 was used to calculate the values of $1/T_m$ shown in the figures.

Tumbling correlation times. X-band CW spectra in 1:1 water:glycerol were obtained at the same temperatures as were used for the SR measurements, and the lineshapes were simulated using the non-linear least square program NLSL[6] to estimate the rotational diffusion rates. The parameters

needed for the NLSL simulations (g_{zz}, g_{yy}, g_{xx}, A_{zz}, A_{yy}, A_{zz}) were obtained by simulating frozen solution spectra, as reported previously.[7] The values used for **1** are $g_{xx} = 2.0092$, $g_{yy} = 2.0057$, $g_{zz} = 2.0024$ and $A_{xx} = 5.9$ G, $A_{yy} = 5.6$ G, $A_{zz} = 36.7$ G. The nitroxyl lineshapes could be fitted well with axial rotation. The tumbling correlation times (τ) were obtained from the rotational diffusion rates using the expression $\tau = \frac{1}{6\sqrt[3]{R_{||}R_{\perp}^2}}$.

Modeling the temperature dependence of $1/T_1$. The signal-to-noise (S/N) per unit time for the pulsed EPR distance measurements depends both on the intensity of the spin echo and on the spin lattice relaxation time, T_1.[7,8] To optimize S/N, a longer spin-lattice relaxation time requires a greater delay between successive DEER or DQC pulse sequences, which decreases the number of scans that can be averaged in a defined period of time. It is therefore important to characterize T_1 as a function of temperature.

As previously described,[1,9] the temperature dependence of the spin lattice relaxation rates was modeled as the sum of contributions from the Raman,[10] local mode,[11] and tumbling dependent processes which includes modulation of g and A anisotropy,[12-14] and spin-rotation[15] (Figure S1).

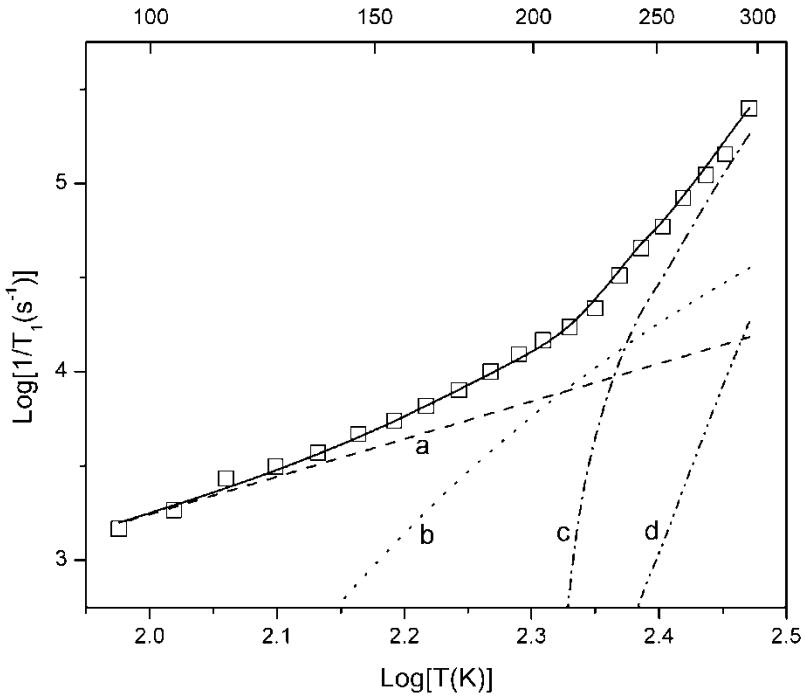

Figure S1. Temperature dependence of electron spin lattice relaxation rates for **1** in 1:1 water:glycerol. The solid line is the sum of contribution from Raman (a), local mode (b), modulation of g and A anisotropy (c), and spin-rotation (d) processes.

The temperature dependence of $1/T_1$ for **1** in 1:1 glycerol:water between 100 and 300 K (Figure S1) is typical of nitroxides.[1,9] Below about 200 K the temperature dependence is characteristic of the Raman process and a local mode, and rates for **1** are slower than for MTSSL by about a factor of 1.6 (Figure S2). At higher temperatures tumbling-dependent processes dominate the relaxation, and rates for **1** are faster than for trihydroxy-DICPO. Solute-solvent interactions are weaker for **1** than for trihydroxy-DICPO,[7] due to the smaller number of hydrogen-bonding sites, which makes tumbling faster, and enhances relaxation.

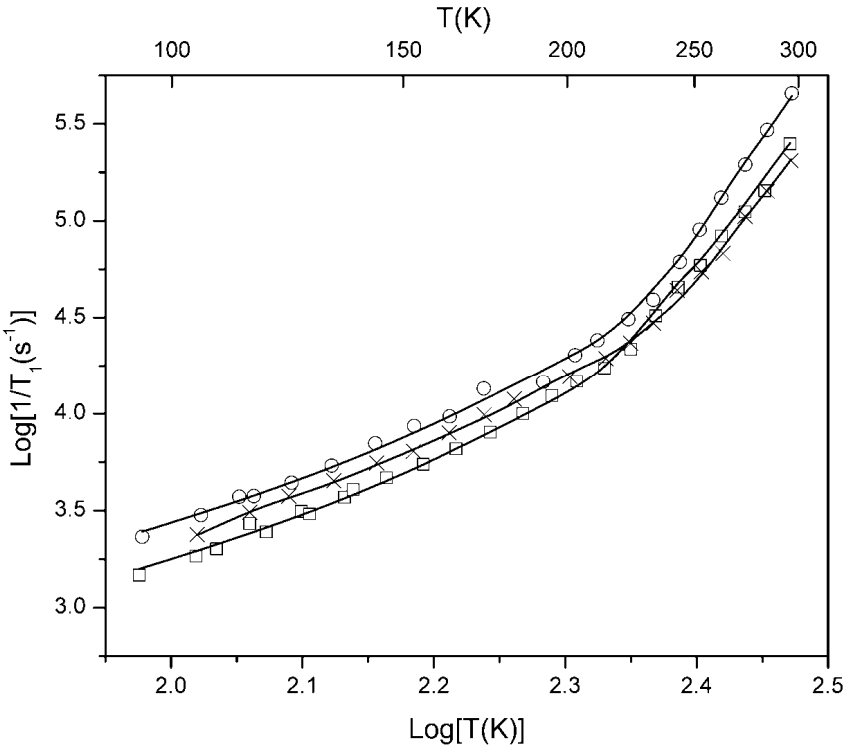

Figure S2. Temperature dependence of electron spin lattice relaxation rate for MTSSL (○) and **1** (□) in 1:1 water:glycerol. The solid lines are the least-squares fits of the relaxation processes to the data. Data for trihydroxy-DICPO [7] are shown for comparison.

Orientation dependence of relaxation. $1/T_m$ and $1/T_1$ at 85 K as a function of position in the spectrum are shown in Figure S3. The linewidths in the spectra of **1** are larger than for MTSSL, which is attributed to unresolved hyperfine couplings to protons of the cyclohexyl groups at positions 2 and 6 of the piperidine ring. Different positions in the CW spectrum correspond to different orientations of the molecule with respect to the external magnetic field. Orientation dependence was studied at 85 K. When there are substantial effects of librations, $1/T_m$ is slower along the principal axes and faster at intermediate orientations.[16,17] The negligible dependence of $1/T_m$ on position in the spectrum is

consistent with the expectation that librations have little impact on dephasing in the rigid 1:1 water:glycerol glass at 85 K.[17,18]

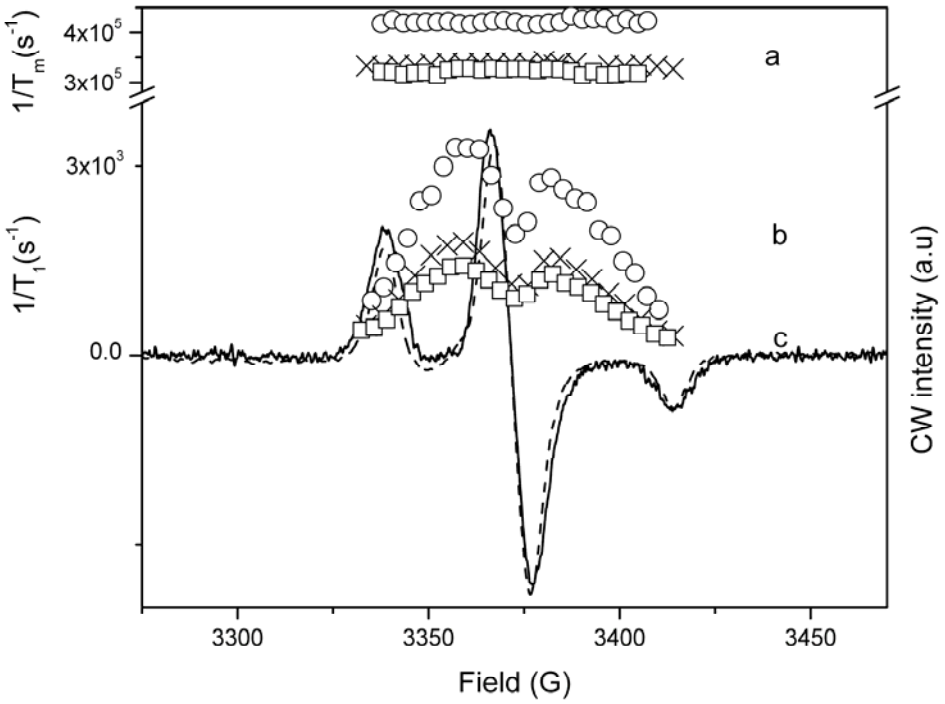

Figure S3. Dependence at 85 K of relaxation rates (a) $1/T_m$ and (b) $1/T_1$ for MTSSL (○), and **1** (□) in 1:1 glycerol:water on position in the CW EPR spectrum (c) for MTSSL (dashed line) and **1** (solid line). Data for trihydroxy-DICPO [7] (×) are shown for comparison.

The spin lattice relaxation rates ($1/T_1$) for **1**, and for MTSSL, depend on position in the spectrum, as has been observed for other nitroxides.[19] At all orientations, relaxation rates for **1** are about 2.3 times slower than for MTSSL.

2. X-ray diffraction.

Crystals of hydantoin nitroxide **3** were grown from various organic solvent mixtures containing ethyl acetate, by slow evaporation of solvents. Typically, two types of crystals were observed, i.e., flat needles and prisms, corresponding to two distinct crystal structures.

Data collection, structure solution, and refinement are briefly summarized below; more detailed description may be found in the crystallographic information files (CIFs). Data were collected at temperature of 100 K at the Advanced Photon Source, Argonne National Laboratory in Chicago, using synchrotron radiation (λ = 0.49595 Å, diamond 1 1 1 monochromator, two mirrors to exclude higher harmonics) with a frame time of 1 s and a detector distance of 6.0 cm were used.

Single crystals were placed onto the tip of an ultra thin glass fiber. The intensity data were corrected for absorption.[20] Final cell constants were calculated from the xyz centroids of strong reflections from the actual data collection after integration.[21]

The space groups P-1 was determined for both structures based on intensity statistics and the lack of systematic absences. Structures were solved with direct methods using Sir2004 and refined with full-matrix least squares / difference Fourier cycles using SHELXL-97.[22,23] All non-hydrogen atoms were refined with anisotropic displacement parameters. The hydrogen atoms were placed in ideal positions and refined as riding atoms with relative isotropic displacement parameters.

Structure A of hydantoin nitroxide 3 (label: 07506). The compound crystallized with two independent molecules per asymmetric unit. The final full matrix least squares refinement converged to R1 = 0.0429 (observed data) and wR2 = 0.1408 (F^2, all data). The remaining electron density is

negligible and located on bonds (0.501 and –0.442 e $Å^{-3}$). In structure A, molecule A and symmetry equivalents form a separate hydrogen bonding network from that of molecule B and its symmetry equivalents (Table S1, Figure S4).

Structure B (solvent polymorph of A) of hydantoin nitroxide 3 (label: 07507). The compound crystallized with two independent molecules in the asymmetric unit and one half solvent molecule (ethyl acetate) per asymmetric unit. The solvent molecule was disordered over two sites. The final full matrix least squares refinement converged to R1 = 0.0431 (observed data) and wR2 = 0.1462 (F^2, all data). The remaining electron density is negligible and located near the disordered solvent and on bonds (0.467 and –0.461 e $Å^{-3}$). In structure B, molecule A and B, and their symmetry equivalents, form hydrogen bonds to each other (Table S2, Figure S5).

Table S1. Hydrogen bonds for structure A [Å and °] (label: 07506).[a]

D-H...A	d(D-H)	d(H...A)	d(D...A)	<(DHA)
N1A-H1NA...O3A#1	0.88	2.00	2.8255(14)	154.7
N2A-H2NA...O2A#2	0.88	2.04	2.8705(15)	157.6
N1B-H1NB...O3B#1	0.88	1.97	2.7567(14)	148.4
N2B-H2NB...O2B#3	0.88	2.06	2.8261(15)	145.3

[a] Symmetry transformations used to generate equivalent atoms: #1 x+1,y,z; #2 -x+1,-y,-z+1; #3 -x+2,-y,-z+2

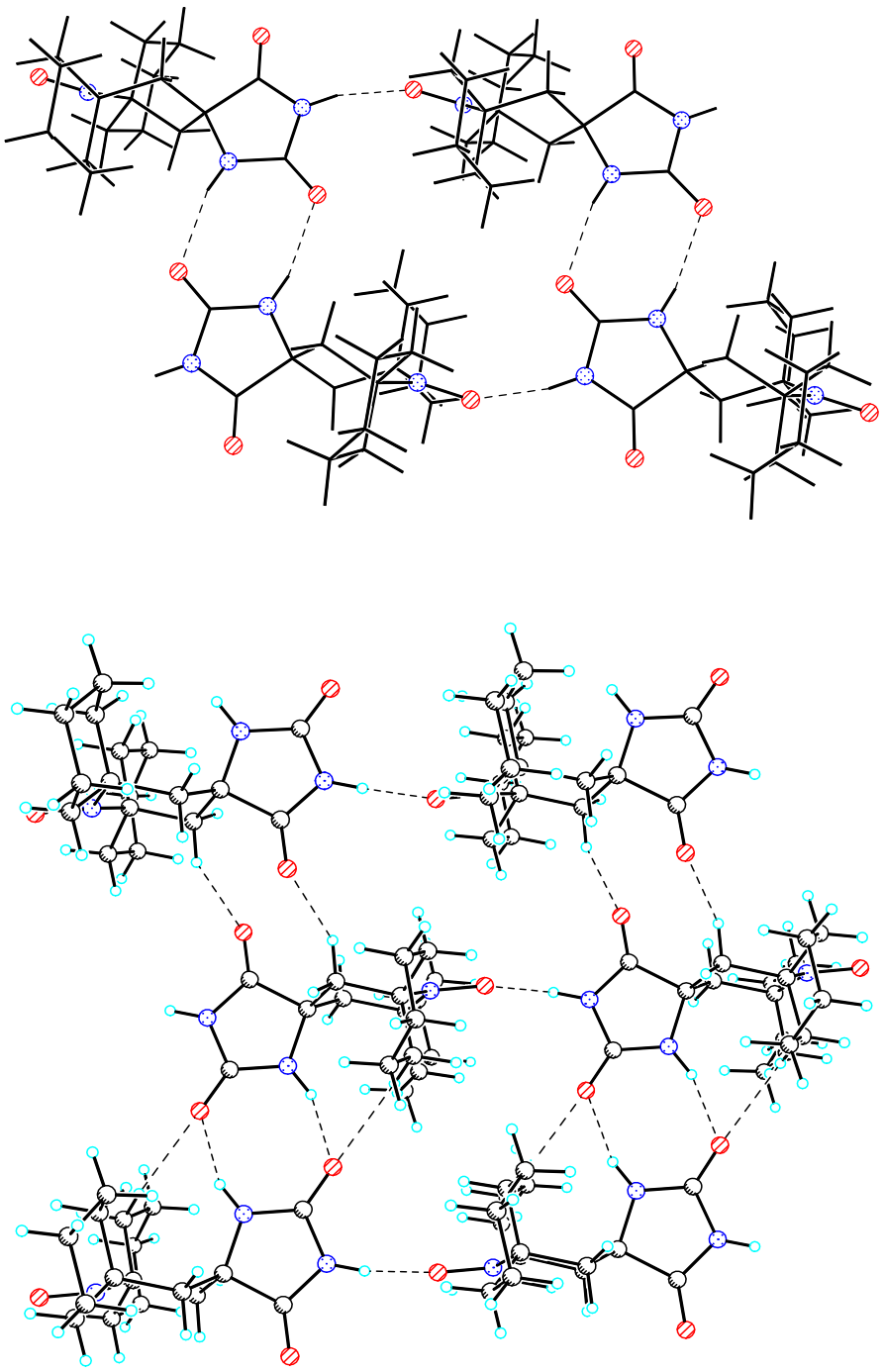

Figure S4. Hydrogen bonding in structure A (label: 07506). Top: molecule A and symmetry equivalents; only classical H-bonding is observed. Bottom: molecule B and symmetry equivalents; both classical and non-classical H-bonding is observed.

Table S2. Hydrogen bonds for structure B [Å and °] (label: 07507).[a]

D-H...A	d(D-H)	d(H...A)	d(D...A)	<(DHA)
N1A-H1NA...O3A#1	0.88	2.00	2.8386(16)	159.7
N2A-H2NA...O2B#1	0.88	1.95	2.7991(14)	161.5
N1B-H1NB...O3B#2	0.88	1.95	2.7335(16)	146.8
N2B-H2NB...O2A#2	0.88	2.08	2.9183(14)	158.2

[a] Symmetry transformations used to generate equivalent atoms: #1 x-1,y,z; #2 x+1,y,z

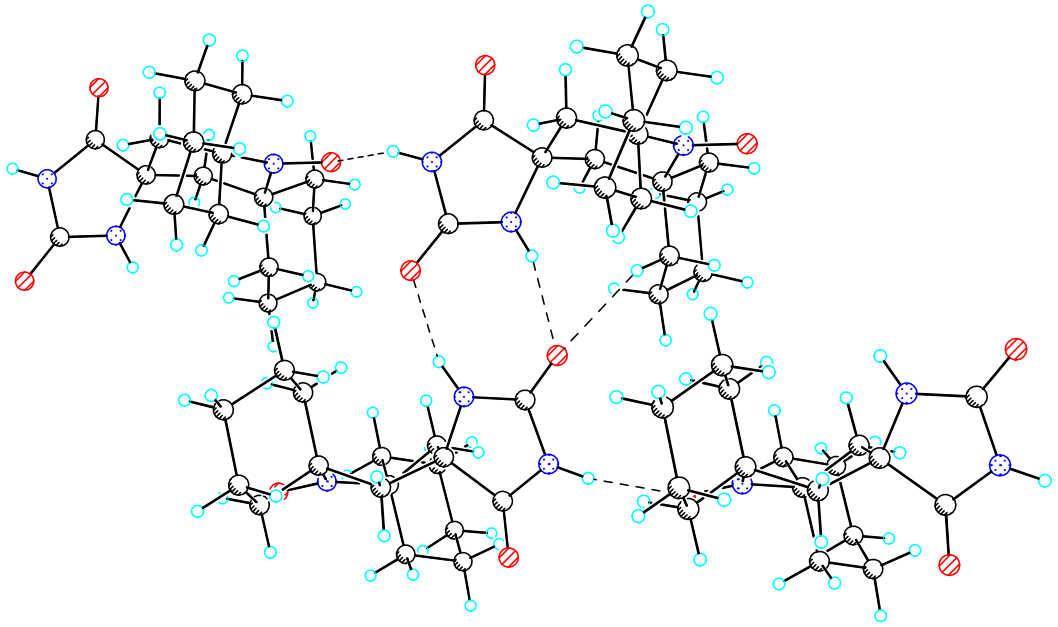

Figure S5. Hydrogen bonding in structure B (label: 07507). Top: molecule A and B, and their symmetry equivalents; both classical and non-classical H-bonding is observed.

3. Detailed experimental procedures for synthesis of α-amino acid nitroxide 1 and Fmoc-1.

General procedures and materials. Column chromatography was carried out on TLC grade silica gel (Aldrich) or flash silica, using 0–20 psig pressure. Preparative TLC (PTLC) was carried out using Analtech silica plates (tapered with a preadsorbent zone). Selected amino acid samples, obtained by

direct hydrolysis of hydantoin, were filtered through Dowex (50W-hydrogen, 8% cross-linking, 100–200 dry mesh) ion-exchange resin (washing with water, followed by 1 M solution of NH_4OH). Purified water (17 MΩ-cm) was obtained from an ultra pure water system (Nanopure, Barnstead).

Per-deuterated solvents for NMR spectroscopy were obtained from Cambridge Isotope Laboratories. NMR spectra were obtained using Bruker spectrometers (^1H, 500 MHz and 400 MHz), using chloroform-*d*, dimethyl sulfoxide-d_6, and water-d_2 (D_2O) as solvents. The 500-MHz spectra for nitroxide radicals were obtained at 298.0 K using cryoprobe. The chemical shift references were as follows: ^1H, chloroform-*d*, (7.260 ppm, $CHCl_3$), dimethyl sulfoxide-d_6, (2.500 ppm, CD_3SOCD_2H), water-d_2 (4.800 ppm, HDO); ^{13}C, chloroform-*d* (77.00 ppm, $CDCl_3$). Typical 1D FID was subjected to exponential multiplication with an exponent of 0.3 Hz (for ^1H) and 1.0–2.0 Hz (for ^{13}C). For ^1H spectra of concentrated solutions of nitroxides (in 3-mm OD sample tubes), exponents of 0.3–12 Hz were used; the spectra were plotted with reference to the residual solvent peaks, without correction for bulk paramagnetic susceptibility.

IR spectra were obtained using a Nicolet Avatar 360 FT-IR instrument, equipped with an ATR sampling accessory (Spectra Tech, Inc.). Compound (solid or as solution in CH_2Cl_2) was applied to the surface of a ZnSe ATR plate horizontal parallelogram (45°, Wilmad). After the solvent evaporated, the spectrum was acquired.

MS analyses were carried out at the Nebraska Center for Mass Spectrometry.

Synthetic details.

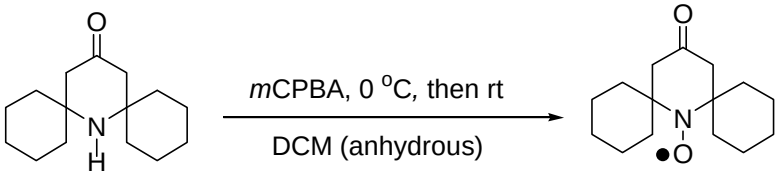

2

Table S3. Ketone nitroxide **2**.

Reaction	Aminoketone g/mmol	*m*CPBA mg/mmol	Target material		
			^{1}H NMR	Amount (g)	Yield (%)
SKR0130[a]	0.030/0.127	44/0.255	skr01030-2nd	0.0064	20
SKR0136	0.042/0.178	68/0.393	skr0136-col	0.0235	53
SKR0140	0.175/0.744	283/1.64	skr0140-pdt	0.071	38
SKR0207	0.515/2.19	794/4.60	skr0207-pdt	0.315	57
xsz-3-70	0.623/2.65	962.2/5.58	xsz-3-70-col	0.3336	50
SS05-48	0.3654/1.555	0.5635/3.265	SS05-48-fr3	0.2815	72
SS05-54	0.6490/2.762	1.0009/5.799	SS05-54-fr3	0.4528	66
SS05-55	0.6447/2.743	1.4202/8.229	SS05-55-fr3	0.8636	71
	0.4362/1.856	0.9609/5.568			
SS05-57	1.3028/5.544	2.3917/13.859	SS05-57-fr3a SS05-57-fr3b	0.8010	58
SS05-61	1.000/4.255	1.8359/10.638	SS05-61-fr2, 0.261 g SS05-61-fr3, 0.238 g SS05-61-fr4, 0.0586 g	0.558	53

[a] Throughout the following paragraphs describing synthesis, labels "SKR0130", "xsz-3-70", and alike correspond to sample or experiment codes directly traceable to the laboratory notebooks or raw data.

Ketone nitroxide 2. Solution of *m*CPBA (0.794 g, 4.60 mmol, 2.1 equiv, SKR0125, MW 172.57) in DCM (15 mL) was added dropwise over 30 min to a solution of the starting aminoketone (0.515 g, 2.19 mmol, 1 equiv, SKR0177-up-2nd, MW 235) in DCM (45 mL) at 0 °C under N_2 atmosphere. The reaction mixture was stirred at 0 °C under N_2 atmosphere. After monitoring by TLC (silica, 30% ethyl acetate in hexane) showed that the starting material was undetectable after stirring for about 90 min at 0 °C, the volume of DCM was reduced and the reaction mixture was extracted with ether. The

ether layer was washed 2 times with $NaHCO_3$ (10%) brine solution, and then dried over Na_2SO_4; concentration of the ether extract under vacuum gave the crude product (0.631 g, SKR0207-crd). Column chromatography (silica, gradient elution with 0-12% ethyl acetate in hexane) gave the product (0.316 g, 57%, SKR0207-pdt). Mp: 111–113 °C (recrystallized from ethanol, SKR0140-pdt/SS0445-sld) (lit.[24] 114–116 °C). EPR (X-band, 9.4817 GHz, chloroform, SKR0140-pdt): a_N = 1.47 mT. LR-FABMS (gly matrix, SKR0140-pdt): *m/z* ion type (%RA = percent relative amplitude for *m/z* = 200–1000), 252.2 $[M+2H]^+$ (100). LR/HR-FABMS (3-NBA matrix, SKR0140-pdt): *m/z* ion type (%RA = percent relative amplitude for *m/z* = 100–1000, deviation from formula), 251.1950 $[M+2H]^+$ (36, 5.4 ppm for $^{12}C_{15}{}^{1}H_{26}{}^{14}N_1{}^{16}O_2$), 251.1884 $[M+H]^+$ (100, 0.5 ppm for $^{12}C_{15}{}^{1}H_{25}{}^{14}N_1{}^{16}O_2$), 250.1808 $[M]^+$ (83, –0.4 ppm for $^{12}C_{15}{}^{1}H_{24}{}^{14}N_1{}^{16}O_2$). IR (ZnSe, cm^{-1}, SKR0140-pdt): 2960, 2934, 2920, 2867, 1719 ($\nu_{C=O}$), 1455, 1405, 1322, 1294, 1258, 1209, 710.

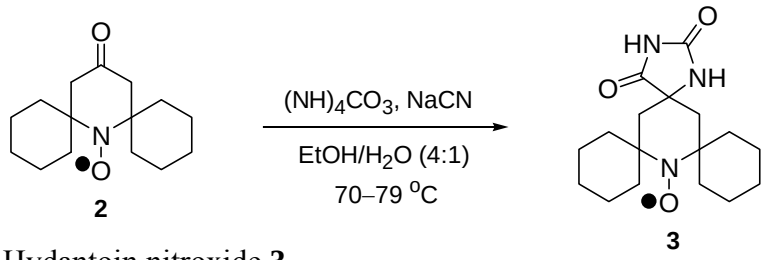

Table S4. Hydantoin nitroxide **3**.

Run	SM mg/mmol	$(NH_4)_2CO_3$ g/mmol	NaCN g/mmol	EtOH/H_2O	Temp (°C)	Target material		
						Sample label	Amount (g)	Yield (%)
SKR0138	0.013/0.052	0.050/0.52	0.010/0.21	1:1	50-55	skr01038-6th spt	0.0022	13
SKR0148	0.016/0.064	0.092/0.96	0.025/0.51	4:1	70-75	skr0148-pdt	0.0091	44
SKR0158	0.031/0.123	0.177/1.84	0.042/0.86	4:1	70-75	skr0158-pdt	0.023	58
SKR0212	0.150/0.6	1.267/13.2	0.294/6.00	4:1	70-75	skr0212-res-2	0.102	69
						skr0212-res-3	0.030	
xsz-3-46	0.158/0.63	1.337/13.9	0.308/6.28	4:1	~77	xsz-3-46-solid1	0.1982[a]	98
xsz-3-71	0.157/ 0.63 0.157/ 0.63	1.328 /13.8 1.328/13.8	0.309/6.30 0.309/6.30	4:1 4:1	~79 ~79	xsz-3-71-crd1	0.4093[a]	~100
SS04-03	0.0300/0.120	0.253/2.64	0.059/1.20	4:1	70-75	SS04-03-cr1, SS04-03-cr2, SS04-03-cr3	0.0237	78
SS05-41	0.2794/1.118	2.360/24.58	0.548/11.18	4:1	70-75	SS05-41-cr1, SS05-41-cr2	0.4368	~100
SS05-58	0.4528/1.811	3.825/39.85	0.888/18.11	4:1	70-75	SS05-58-sld1, SS05-58-cr2	0.5966	98
SS05-60	0.9900/3.960	8.363/87.12	1.940/39.59	4:1	70-75	SS05-60-cr1cr2	1.2009	95

[a] The samples of hydantoin nitroxide **3** in the runs labeled as xsz-3-46 and xsz-3-71 contain residual solvent (chloroform), as indicated by the ^{1}H NMR spectra (e.g., Figure S14); therefore, the actual yields are slightly lower for these two runs.

Hydantoin nitroxide 3. Solution of $(NH_4)_2CO_3$ (1.267 g, 13.2 mmol, MW 96) in distilled water (5 mL) and solution of NaCN (0.294 g, 6.00 mmol, MW 49) in distilled water (2 mL) were added to a solution of ketone nitroxide **2** (0.150 g, 0.600 mmol, MW 250, SKR0207-pdt) in ethanol (35 mL). After both additions, the reaction mixture appeared hazy. Thus, water (~3 mL), followed by ethanol

(~5 mL) were added, to provide the reaction mixture as a clear solution. Subsequently, the mixture was stirred at 73–75 °C. After 20 h at 73–75 °C, TLC analysis (silica, 50% ethyl acetate in hexane) showed presence of starting material and hydantoin nitroxide **3**. At this time, additional amount of $(NH_4)_2CO_3$ (~100 mg) and NaCN (~20 mg) were added as solution in water. After additional 15 h at 73–75 °C (total of 35 h), the reaction was allowed to attain room temperature, and then extraction with ethyl acetate was carried out three times. The ethyl acetate layers were washed with water and brine, dried over Na_2SO_4, and then concentrated in vacuo at 45 °C, to provide crude product (0.186 g, SKR0212-crd). The crude product was dissolved in a minimum volume of chloroform. After two days of slow evaporation at room temperature, the product as a pink precipitate was filtered off from the wine colored mother liquor. The process was repeated. The two crops (0.120 g and 0.0305 g, SKR0212-res-2 and SKR0212-res-3) corresponded to 69% yield of **3**. The isolated yields can be improved by more exhaustive precipitations, starting with dissolution of the crude product in hot chloroform.

Mp: 241–242 °C (dec) (SS04-03-cr2). EPR (X-band, 9.4893 GHz, 297 K, ethanol, xsz-371-crd1): a_N = 1.51 mT. Spin concentration (EPR): 93% (xsz-371-crd1); the spin concentration is somewhat lower due to the presence of residual solvent (chloroform), as indicated by ^{1}H NMR spectra (Fig. S12). LR-FABMS (gly matrix, skr0138-6th): *m/z* 322 $[M+2H]^+$. LR/HR-FABMS (gly matrix, xsz-371-crd1): *m/z* ion type (%RA = percent relative amplitude for *m/z* = 200–1500, deviation from formula), 322.2126 $[M+2H]^+$ (100, 1.5 ppm for $^{12}C_{17}{}^{1}H_{28}{}^{14}N_3{}^{16}O_3$); (gly matrix, SS04-03-cr2): *m/z* ion type (% RA = percent relative amplitude for *m/z* = 200–800, deviation from formula), 322.2137 $[M+2H]^+$ (100,

–2.1 ppm for $^{12}C_{17}{}^{1}H_{28}{}^{14}N_3{}^{16}O_3$). IR (ZnSe, cm^{-1}, SKR0138-6th-r2): 3237, 2927, 2858, 2361, 2332, 1771, 1722, 1683, 1447, 1407, 1239.

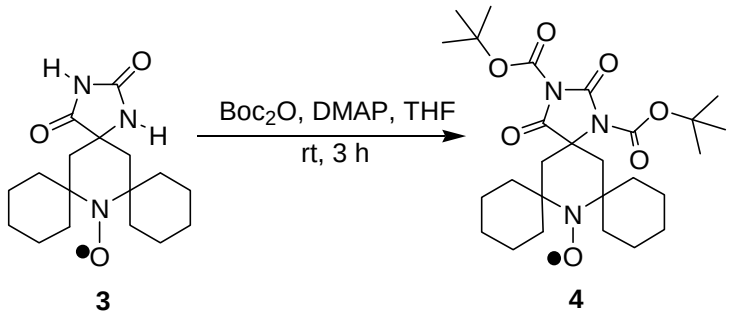

3 **4**

Table S5. Di-Boc hydantoin nitroxide **4**.

Run	Hydantoin nitroxide **3** g/mmol	Boc_2O (1.0 M in THF) mL/mmol	DMAP (in THF)[a] mL (conc., M) / mmol	Target Material	
				Yield mg (%)	Sample label
SS03-72	0.0100/0.031	0.1/0.1	0.022 (0.14 M) / 0.0031	15.7 (97)	SS03-72
SS03-74	0.0199/0.062	0.2/0.2	0.044 (0.14 M) / 0.0062	22.6 (70)	SS03-74
SS04-68	0.0406/0.126	0.4/0.4	0.081 (0.14 M) /0.0130	64.7 (98)	SS04-68
SS05-67	0.1012/0.3160	1.0/1.0	0.112 (0.28 M) / 0.0316	117.9 (72)	SS05-67-fr3
SS05-71	0.1527/0.954	2.9/2.9	0.340 (0.28 M) / 0.0954	174.6 (70)	SS05-71-fr4
SS05-77	0.260/0.812	2.5/2.5	0.288 (0.28 M) / 0.0812	284.3 (67)	SS05-77-fr4
SS05-91	0.320/0.999	3.0/3.0	0.244 (0.41 M) / 0.0999	352.8 (68)	SS05-91-fr3fr4

[a] Small volumes of the DMAP (dimethylaminopyridine) solution were measured by counting drops using calibrated needle-syringe.

Di-Boc hydantoin nitroxide 4. Hydantoin nitroxide **3** (19.9 mg, 0.062 mmol, MW = 320.21) was evacuated for 30 min in a Schlenk vessel on a vacuum line, and then THF (1.0 mL, distilled from Na/ benzophenone) was added to the Schlenk vessel under nitrogen. The resultant yellow orange colored solution was stirred vigorously, and then Boc_2O (0.2 mL, 1.0 M in THF, 0.2 mmol), followed by DMAP (0.044 mL, 0.14 M in THF, 0.0062 mmol) were added dropwise via a syringe. Vigorous

bubbling was observed, presumably due to evolution of carbon dioxide. The reaction was monitored by TLC (silica, R_f = 0.37 for di-Boc-hydantoin **4** in 20% diethyl ether in pentane and R_f = 0.38 for hydantoin **3** in 40% ethyl acetate in pentane). After 3 h at room temperature, the reaction mixture was transferred to a vial using diethyl ether, and then concentrated under nitrogen gas flow. The concentrated solution was applied on a short plug of silica gel (ca. 3-cm length), and then eluted with pentane (3 × 20 mL), to remove excess Boc_2O and vacuum grease, followed by 30% diethyl ether in pentane (6 × 20 mL). Concentration *in vacuo* (diaphram pump and then overnight on a high vacuum line in a Schlenk-like container) gave the product (SS03-74) as a yellow solid (22.6 mg, 70%). Mp: 130–131 °C (SS03-74). EPR (X-band, 9.4901 GHz, ethanol, 296 K, SS03-74, SKR264r2): a_N = 1.60 mT. LR/HR-FABMS (3-NBA matrix, SS03-74): m/z ion type (% RA = percent relative amplitude for *m/z* = 300–1000, deviation from formula), 522.3188 $[M+2H]^+$ (100.0, –1.6 ppm for $^{12}C_{27}{}^{1}H_{44}{}^{14}N_3{}^{16}O_7$). IR (ZnSe, cm^{-1}, SS03-74): 2983, 2934, 2861, 1827, 1782, 1747, 1459, 1370, 1309, 1252, 1145, 845, 760.

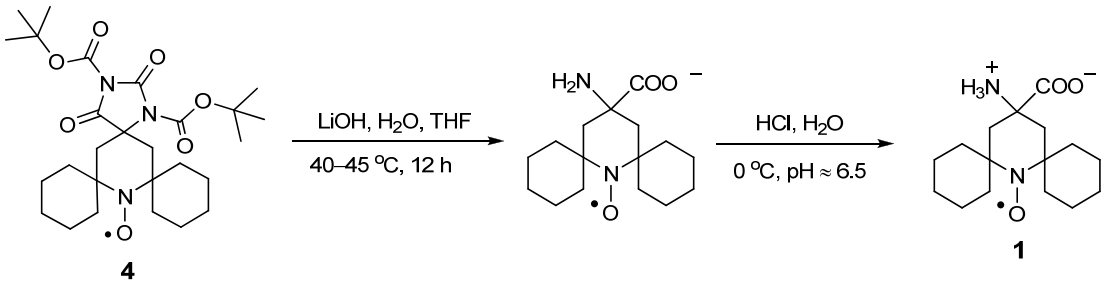

4 **1**

Table S6. Amino acid nitroxide **1**.

Run	Starting material		2.0 M aq. LiOH solution	Target material		
	mg / mmol)	Sample label	mL (conc., M) / mmol	Yield mg (%)	Sample label	LR/HR-FABMS (gly matrix): *m/z* ion type (% RA for *m/z* = 200–1200, dev from formula)
SS03-77	15.7/0.030	SS03-72	0.1 (2.0)/0.2	0.8 (09)	SS03-77-pdt1a	297.2175 $[M+2H]^+$ (100, 1.2 ppm for $^{12}C_{16}{}^{1}H_{29}{}^{14}N_2{}^{16}O_3$)
SS03-91	14.6/0.028	SS03-74	0.1 (2.0)/0.2	4.4 (53)	SS03-91-pdt 1b	297.2178 $[M+2H]^+$ (100, 0.1 ppm for $^{12}C_{16}{}^{1}H_{29}{}^{14}N_2{}^{16}O_3$)
SS04-74	63.8/0.123	SS04-68	0.5 (2.0)/1.0	16.6 (46)	SS04-74-zwAmAc	297.2175 $[M+2H]^+$ (100, 1.0 ppm for $^{12}C_{16}{}^{1}H_{29}{}^{14}N_2{}^{16}O_3$)
SS05-65	177.2/0.341	SS05-67-fr3 SS05-51-fr4	2.7 (1.0)/2.7	77.4 (77)	SS05-65-am ac	297.2179 $[M+2H]^+$ (100, –0.4 ppm for $^{12}C_{16}{}^{1}H_{29}{}^{14}N_2{}^{16}O_3$)
SS05-84	284.3/0.547	SS05-77-fr4	4.4 (0.99)/4.4	71.5 (45)	SS05-84-sld1 SS05-84-sld2	HR-FABMS not taken.
SS06-02	174.6/0.336	SS05-71-fr4	3.0 (0.99)/3.0	51.1 (52)	SS06-02-sld2	HR-FABMS not taken.
SS06-31	376.0/0.723	SS05-79-fr2	8.0(1.014)/8.1	125.8 (59)	SS06-31-sld1	LR-FABMS only.

Amino acid nitroxide 1. Nitroxide **4** (14.6 mg, 0.028 mmol, label: SS03-74, MW = 520.23) was evacuated in a Schlenk vessel for overnight. THF (0.1 mL) was added to the Schlenk vessel under nitrogen. To the resultant yellow homogeneous solution, stirred vigorously, aqueous lithium hydroxide solution (2.0 M, prepared using purified water) was added. The mixture was stirred overnight at 40–45 °C under nitrogen atmosphere. Subsequently, the reddish brown colored THF phase (the top layer) was pipetted out from the Schlenk vessel and the aqueous phase was extracted

with diethyl ether (8 × 0.2 mL). The combined THF and ether layers were concentrated in vacuo to provide a light yellow solid (7.6 mg, SS03-91-org).

The light yellow aqueous layer was flushed with nitrogen gas to remove residual diethyl ether, and then transferred to a centrifuge tube. Subsequently, the aqueous layer was titrated at 0 ^{o}C with 6.0 M and 2.0 M hydrochloric acid (and 2.0 M LiOH, as needed) using pipette, until the pH of 6.5 was reached. The resultant light yellow solid was collected by repetitive centrifugation and treatment with purified water (6 × 0.2 mL), and then by drying under nitrogen gas flow. The solid was further dried using the diaphram pump. Further removal of water was carried out by several treatments with anhydrous ethanol (5 × 0.2 mL), followed by drying the solid under the nitrogen flow, and then using the diaphragm pump. The yellow solid (4.6 mg, SS03-91-pdt1) thus obtained was transferred from the centrifuge tube to a vial and further dried in an evacuation container in 10 mTorr vacuum at 70 ^{o}C for 48 h. The product **1** was obtained as a yellow solid (4.4 mg, SS03-91-pdt1b). Because of low solubility in water for zwitterionic form of **1**, ^{1}H NMR spectra were obtained in solutions of LiOH in D_2O.

Zwitterionic form of 1. Mp: 211–213 °C (SS03-91-pdt1b/SS05-65am ac). EPR (X-band, 9.4917 GHz, 297 K, 0.5 mM in ethanol, SS03-91-pdt1b, SS370r5): a_N = 1.54 mT. LR/HR-FABMS (gly matrix, SS03-91-pdt1b): *m/z* ion type (% RA = percent relative amplitude for *m/z* = 200–1200, deviation from formula), 297.2178 $[M+2H]^+$ (100, 0.1 ppm for $^{12}C_{16}{}^{1}H_{29}{}^{14}N_2{}^{16}O_3$). IR (Zn/Se, cm^{-1}, SS03-91-pdt1b): 3453 (ν_{O-H} of adsorbed, H-bonding H_2O molecules), 3120 (ν_{N-H} of NH_3^+), 2930, 2860,

1597 (ν_{as}, COO^-), 1532, 1448, 1402 (ν_s, COO^-), 1349, 1325, 1312, 1261, 1229, 1178, 1088, 1021, 905, 872, 796, 718.

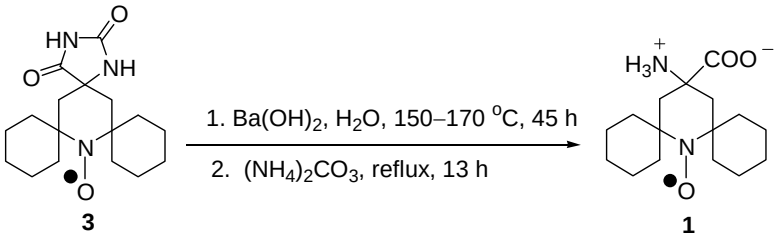

Direct hydrolysis of hydantoin nitroxide 3 to amino acid 1. Solution of barium hydroxide in water was prepared by dissolving $Ba(OH)_2 \bullet 8H_2O$ (20 g) in 25 mL of distilled water at about 80 °C with shaking and sonication, followed by filtering off (with washing using 5 mL of hot water) the insoluble precipitate. A portion of this solution (~0.15 mL, ~0.08 g, ~0.25 mmol) at 85–90 °C was transferred by a hot pipette to hydantoin nitroxide **3** (20 mg, 0.062 mmol, SKR0212-res-3, MW = 320) in a heavy-wall Schlenk vessel. Additional amount of hot distilled water (~1 mL) was added to wash down solid particles into the solution. The reaction mixture was stirred in a sand bath at 150–170 °C for 45 h.

After cooling to room temperature, the cap of the Schlenk vessel was carefully opened and a small portion of the reaction mixture was extracted with ethyl acetate (mini-workup) to check for unreacted starting material; TLC (silica, 50% ethyl acetate in hexane) analyses showed absence of hydantoin nitroxide **3**. Therefore, ammonium carbonate (48 mg, 0.50 mmol) was added to the reaction mixture and a reflux condenser was attached to the Schlenk vessel. The reaction mixture was placed in a sand bath at 150–170 °C and stirred under reflux for 13 h. The reaction mixture was washed with hot distilled water (65 °C) and filtered through sintered funnel. The resultant light pink solution was

washed with ethyl acetate twice, and then the pink aqueous layer was concentrated in *vacuo* at 45 °C to provide the crude product (18.8 mg, SKR0245-crd). EPR (X-band, 9.4955 GHz, 297 K, ethanol, SKR0245-crd): a_N = 1.54 mT. LR/HR-FABMS (3-NBA matrix, SKR045-crd and SKR045-solid): *m/z* ion type (%RA = percent relative amplitude for *m/z* = 200–600, deviation from formula), 297.2188 $[M+2H]^+$ (100, –3.2 ppm for $^{12}C_{16}{}^{1}H_{29}{}^{14}N_2{}^{16}O_3$). LR-FABMS data are shown in Figure S10.

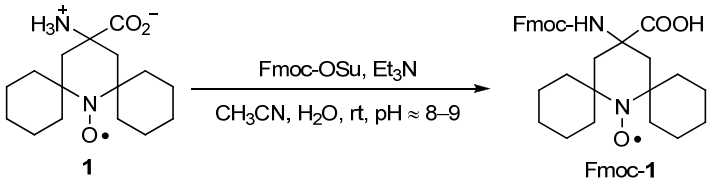

Table S7. Fmoc-amino acid nitroxide Fmoc-**1**.

Run	Starting material		Fmoc-OSu in CH_3CN	Et_3N as aqueous solution	Target material	
	mg/mmol	Sample label	mL (conc., M) / mmol	mL (conc., M) / mmol	Yield mg (%)	Sample label
SS05-88	5.0/0.0169	SS05-84-sld1	0.10 (0.255) / 0.025	0.10 (0.171) / 0.017	1.9 (22)[a]	SS05-88-plc3[b]
SS05-96	25.1/0.084	SS05-84-sld1	0.50 (0.357) / 0.18	0.40 (0.215) / 0.086	24.6(56)	SS05-96-fr3[c]
SS06-06	51.0/0.172	SS06-02-sld	0.75 (0.334) / 0.25	0.80 (0.224) / 0.18	48.9(55)	SS06-06-fr3[d]
SS06-33	125.8/0.426	SS06-31-sld1	1.50 (0.334) / 0.64	1.60 (0.224) / 0.43	125.6 (56)	SS06-33-fr2

[a] In this preliminary run, the product was isolated by preparative TLC. [b] LR/HR-FABMS (gly matrix, SS05-88-plc3): *m/z* ion type (% RA = percent relative amplitude for *m/z* = 150–800, deviation from formula), 519.2852 $[M+2H]^+$ (100, 1.3 ppm for $^{12}C_{31}{}^{1}H_{39}{}^{14}N_2{}^{16}O_5$). [c] LR/HR-FABMS (gly matrix, SS05-96-fr3): m/z ion type (% RA = percent relative amplitude for *m/z* = 150–1200, deviation from formula), 519.2857 $[M+2H]^+$ (100, 0.3 ppm for $^{12}C_{31}{}^{1}H_{39}{}^{14}N_2{}^{16}O_5$). [d] LR/HR-FABMS (gly matrix, SS06-06-fr3): *m/z* ion type (% RA = percent relative amplitude for *m/z* = 150–1050, deviation from formula), 519.2856 $[M+2H]^+$ (100, 0.7 ppm for $^{12}C_{31}{}^{1}H_{39}{}^{14}N_2{}^{16}O_5$).

Fmoc-1. Zwitterionic amino acid nitroxide **1** (25.1 mg, 0.085 mmol, SS05-84-sld1) was added into a vial containing aqueous solution of triethylamine (400 µL of 0.215 M triethylamine solution, 0.086 mmol) and stirred vigorously for 15 min to provide yellow homogenious solution. Fmoc-succinimidyl carbonate (500 µL of 0.357 M solution of Fmoc-Osu in CH_3CN, 0.179 mmol) was

added in two portions with vigorous stirring over 15 min, forming white suspension (pH 8–8.5). Then, additional volume of CH_3CN (100 μL) was added and the reaction mixture was vigorously stirred for additional 30 min, with its progress monitored by TLC ($CHCl_3$/CH_3OH/acetic acid, 9.5 mL : 0.5 mL : 2 drops, R_f = 0.4 for Fmoc-**1**), and additional amount of triethylamine added as needed to maintain basic pH 8–9. Subsequently, the reaction mixture was filtered, concentrated in vacuo, was then poured into cold citric acid solution (1 mL of 20% aqueous citric acid solution). After stirring at 0 ^oC for 15 min, extraction with ethyl acetate (6 × 10 mL) was carried out. The combined ethyl acetate layers were washed with water (3 × 10 mL), and then with brine solution (10 mL), dried over Na_2SO_4, and concentrated under reduced pressure in a rotary evaporator. The yellow crude product (SS05-96-crd, 108.8 mg) was purified by column chromatography (silica gel, 3% methanol in dichloromethane with 0.1% acetic acid). The product was obtained as a yellow polycrystalline solid (24.6 mg, 56%, label: SS05-96-fr3). R_f = 0.33 (3% methanol in dichloromethane with 0.1% acetic acid). Mp: 162–165 ^oC (dec.) (SS06-06-fr3). EPR (X-band, benzene, SS06-06-fr3): g = 2.0060, spin concentration ≈ 100% (vs. tempol in benzene). ^1H NMR (400 MHz, chloroform-*d*, SS05-96-fr3, 10.3 mg in 0.166 mL of chloroform-*d*): δ = 12.72 (br, COOH, exch. D_2O), 7.873, 7.733, 7.503, 4.484, 4.352, 4.248, 3.789, 3.474, 3.195, 2.966, 2.171, 1.728, 1.387, 1.008, 0.198 (grease), and –0.311 (v. br). LR/HR-FABMS (gly matrix, label: SS05-96-fr3): *m/z* ion type (% RA = percent relative amplitude for *m/z* = 150–1200, deviation from formula), 519.2857 $[M+2H]^+$ (100, 0.3 ppm for $^{12}C_{31}{}^1H_{39}{}^{14}N_2{}^{16}O_5$). IR ($cm^{-1}$, ZnSe, sample label: SS05-96-fr3_run6): 3321, 2927, 2858, 1792, 1741, 1519, 1450, 1368, 1303, 1259, 1154, 1085, 1020, 909, 801, 758, 731, 698.

4. LR-FABMS, NMR, and IR spectra for nitroxides.

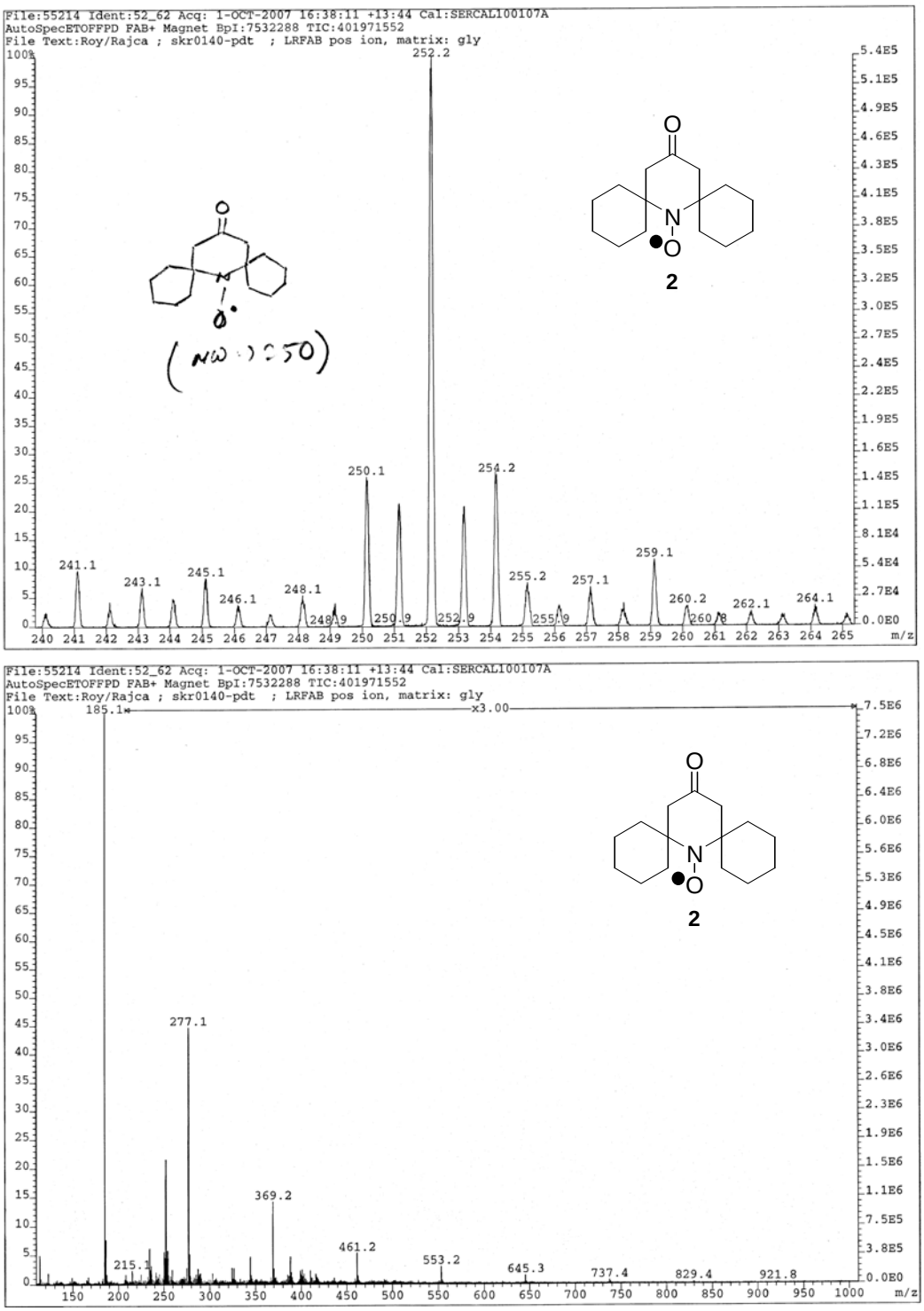

Figure S6. LR-FABMS (gly matrix) of ketone nitroxide **2** (SKR0140-pdt). Top plot: expansion for the $[M+2H]^+$ ion. Bottom plot: full spectrum. Not corrected for the matrix background (*m/z* 185, 277, 369, etc.).

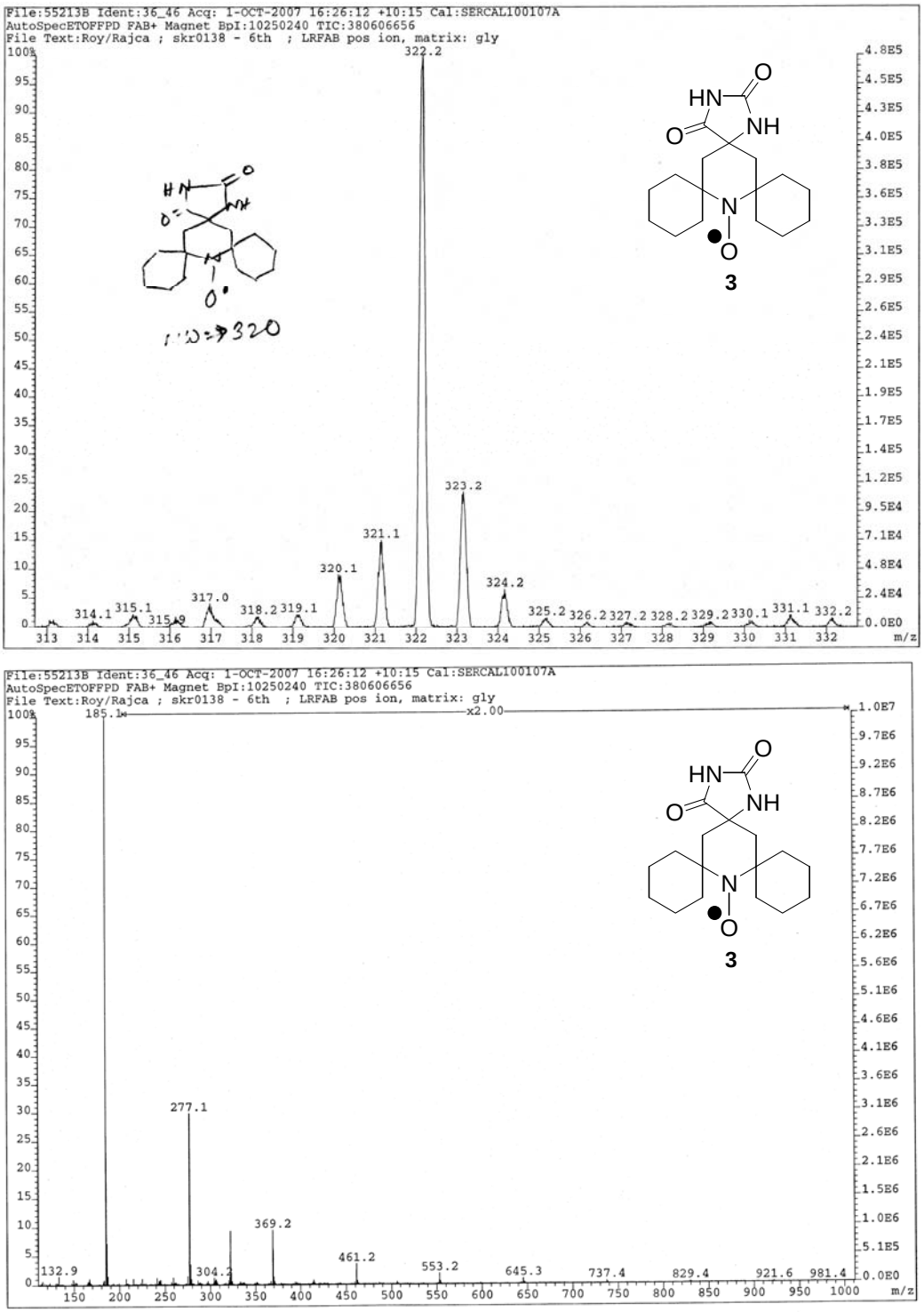

Figure S7. LR-FABMS (gly matrix) of hydantoin nitroxide **3** (SKR0138-6th). Top plot: expansion for the $[M+2H]^+$ ion. Bottom plot: full spectrum. Not corrected for the matrix background (*m/z* 185, 277, 369, etc.).

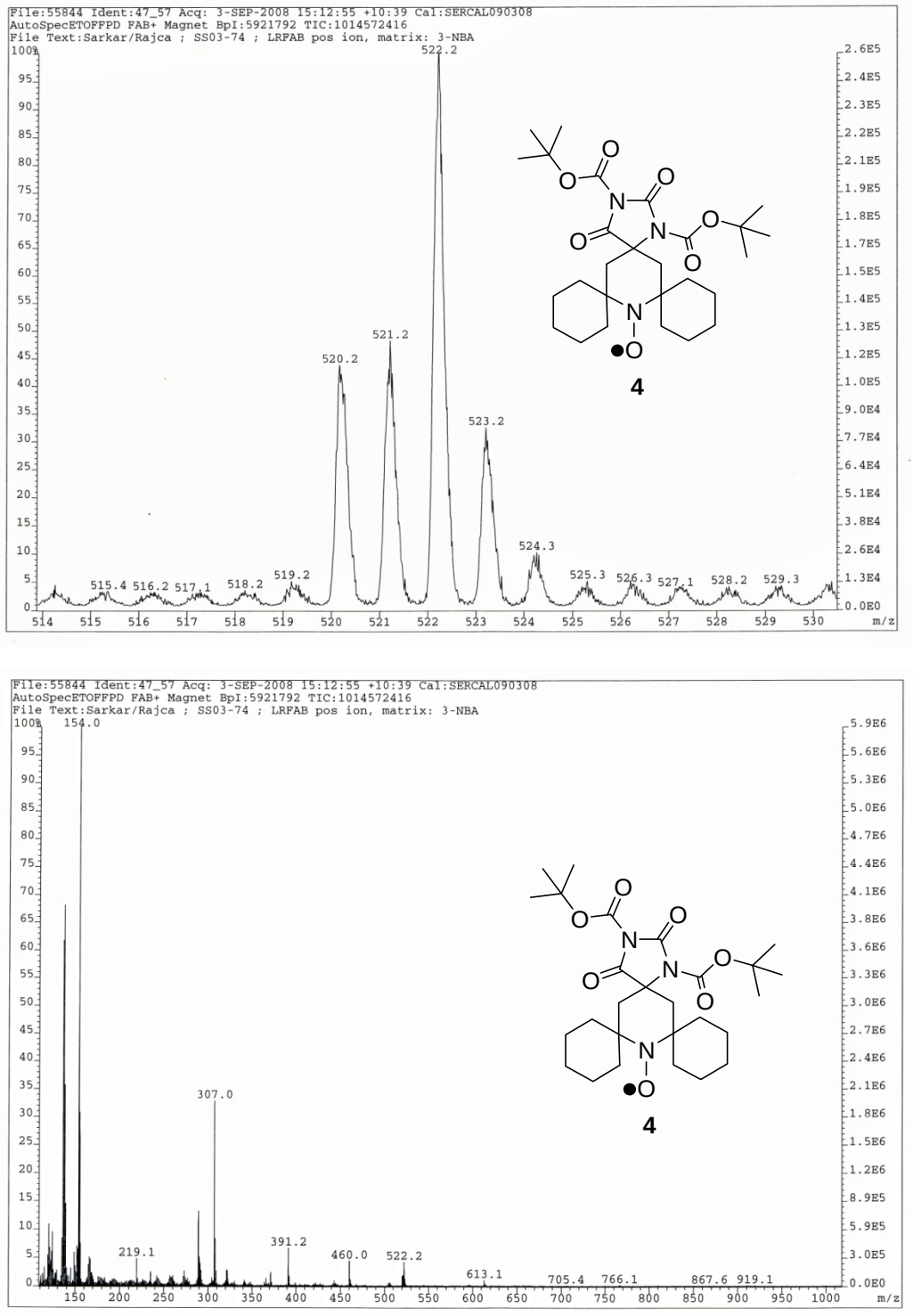

Figure S8. LR-FABMS (3-NBA matrix) of di-Boc hydantoin nitroxide **4** (SS03-74). Top plot: expansion for the $[M+2H]^+$ ion. Bottom plot: full spectrum. Not corrected for the matrix background (*m/z* 136, 154, 289, 307, etc.).

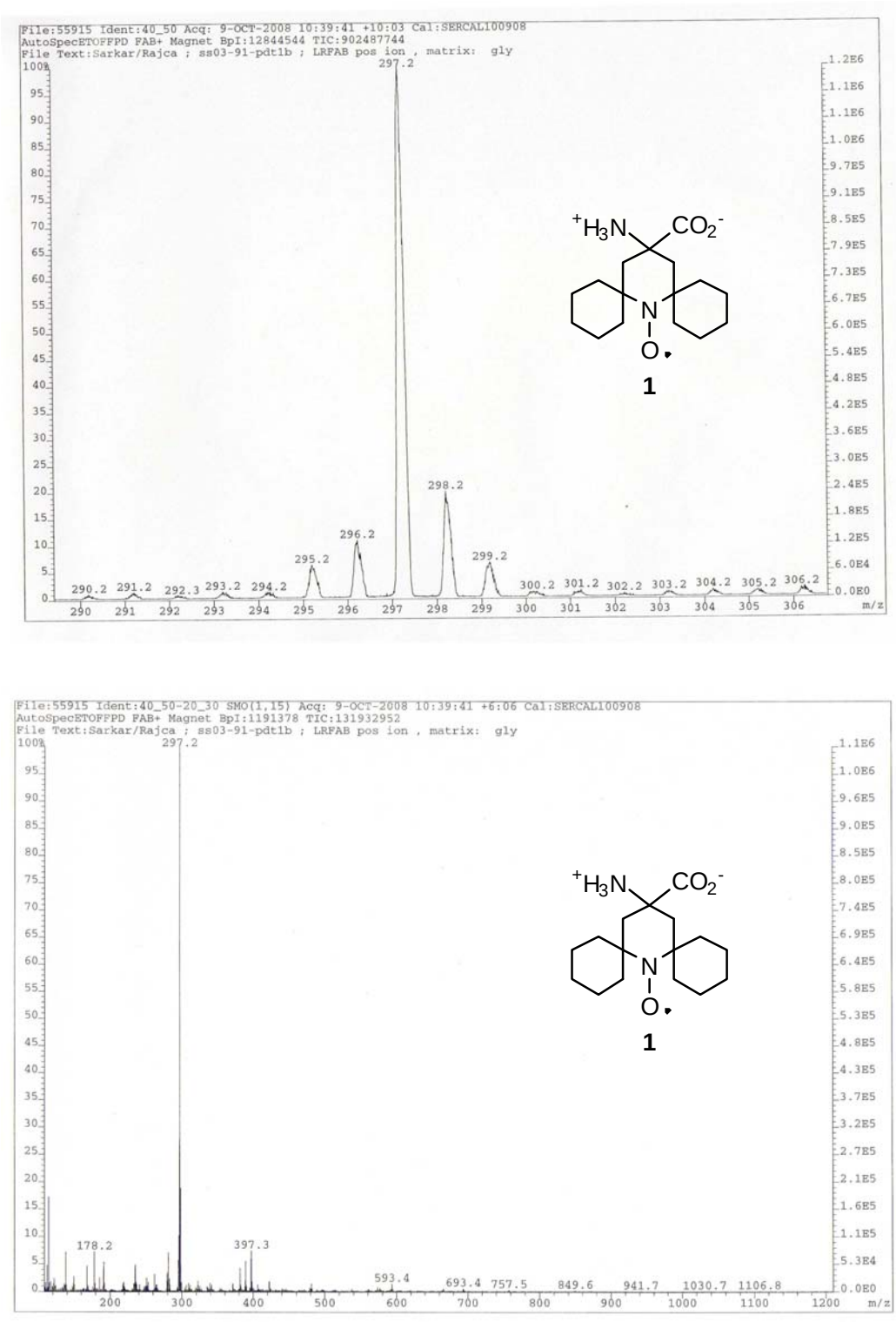

Figure S9. LR-FABMS (gly matrix) of zwitterions amino acid nitroxide **1** (ss03-91-pdt1b). Top plot: expansion for the $[M+2H]^+$ ion. Bottom plot: full spectrum. Corrected for the matrix background.

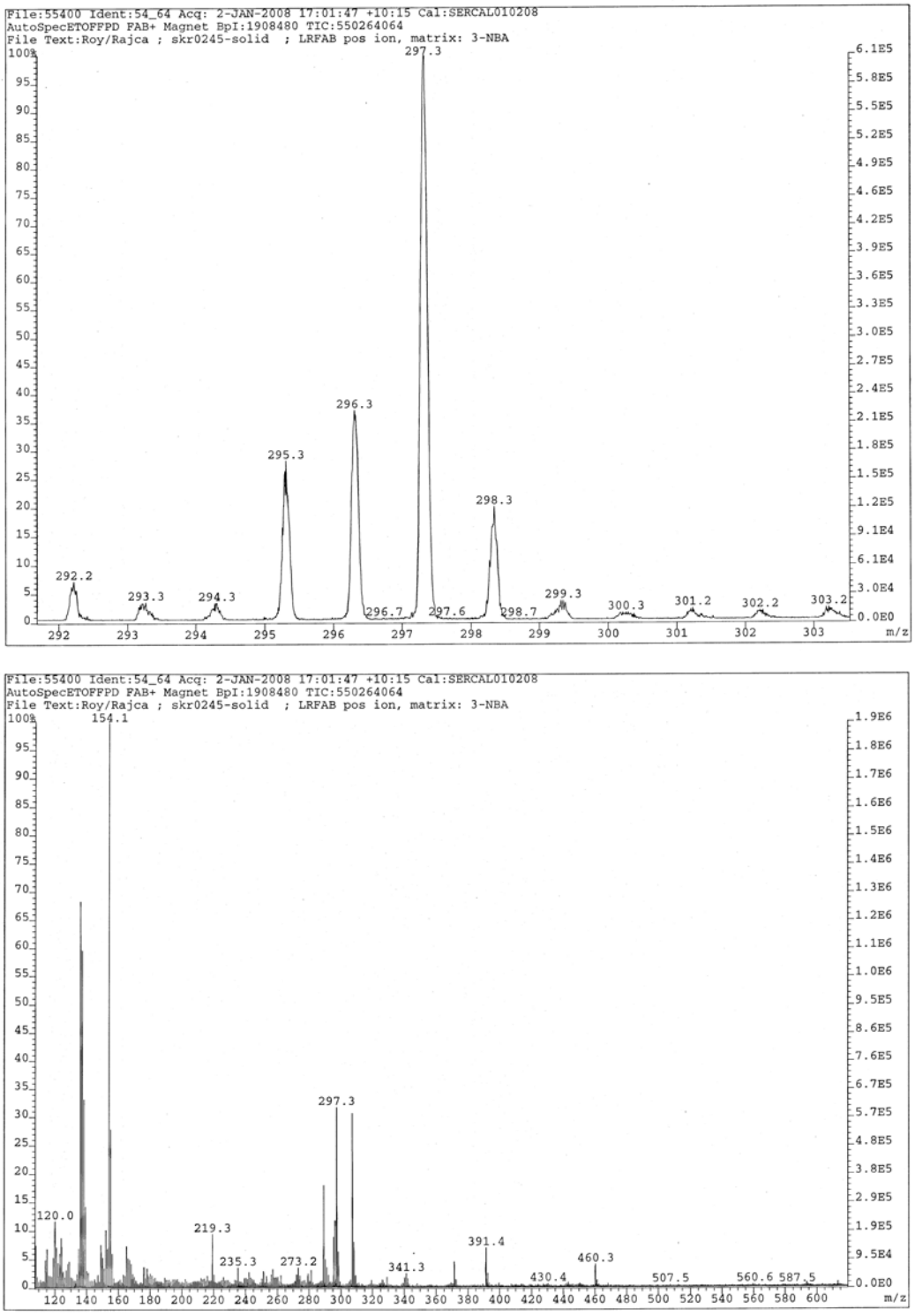

Figure S10. LR-FABMS (3-NBA matrix) of amino acid nitroxide **1** (SKR0245-solid), obtained by direct hydrolysis of hydantoin nitroxide **3**. Top plot: expansion for the $[M+2H]^+$ ion. Bottom plot: full spectrum. Not corrected for the matrix background (*m/z* 136, 154, 289, 307, etc.).

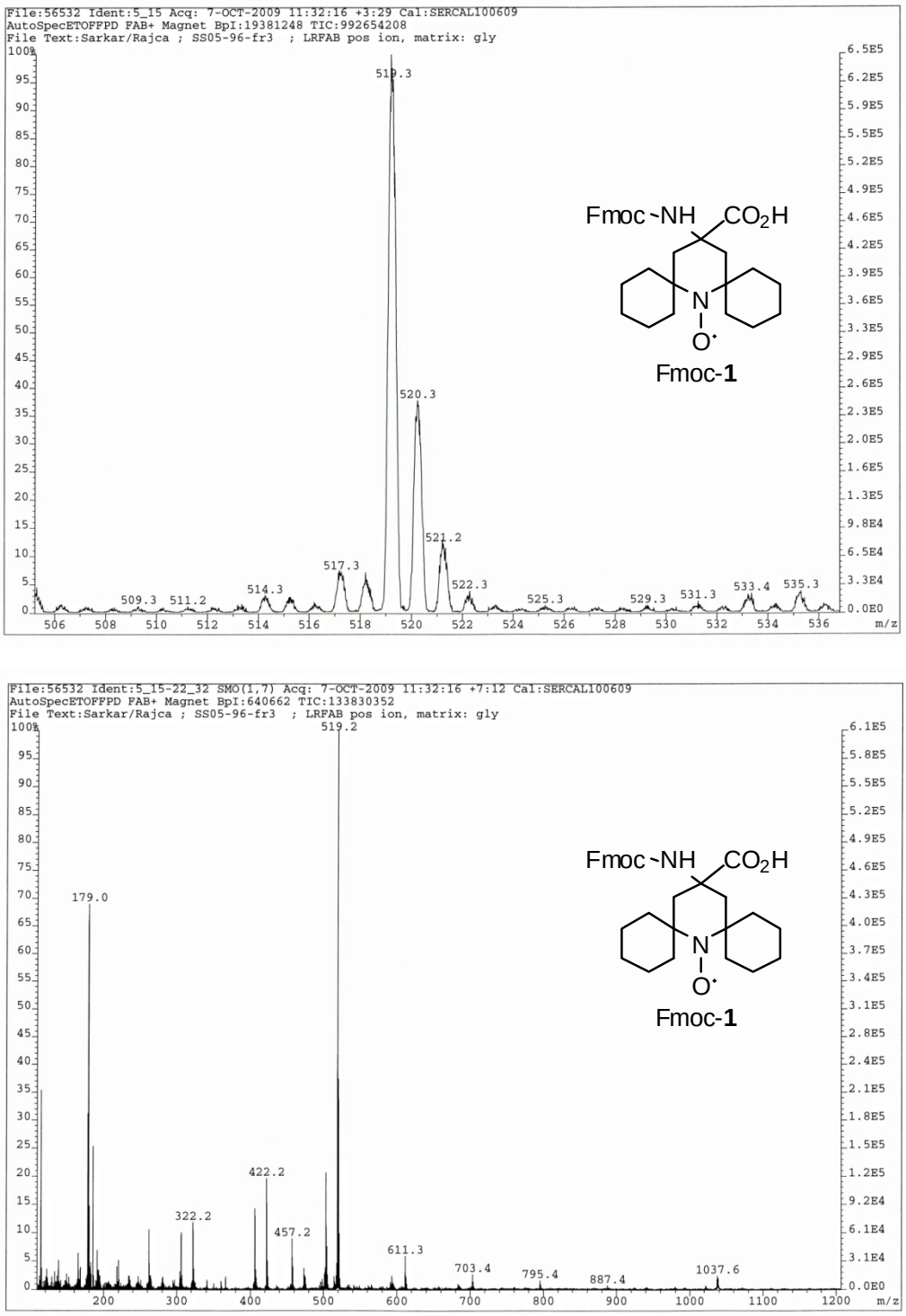

Figure S11. LR-FABMS (gly matrix) of Fmoc-amino acid nitroxide Fmoc-**1** (SS05-96-fr3). Top plot: expansion for the $[M+2H]^+$ ion. Bottom plot: full spectrum. Corrected for the matrix background. Peak at *m/z* 1037.6 is assigned to the $[M+3H]^+$ ion for the carboxylic acid dimer of Fmoc-**1**.

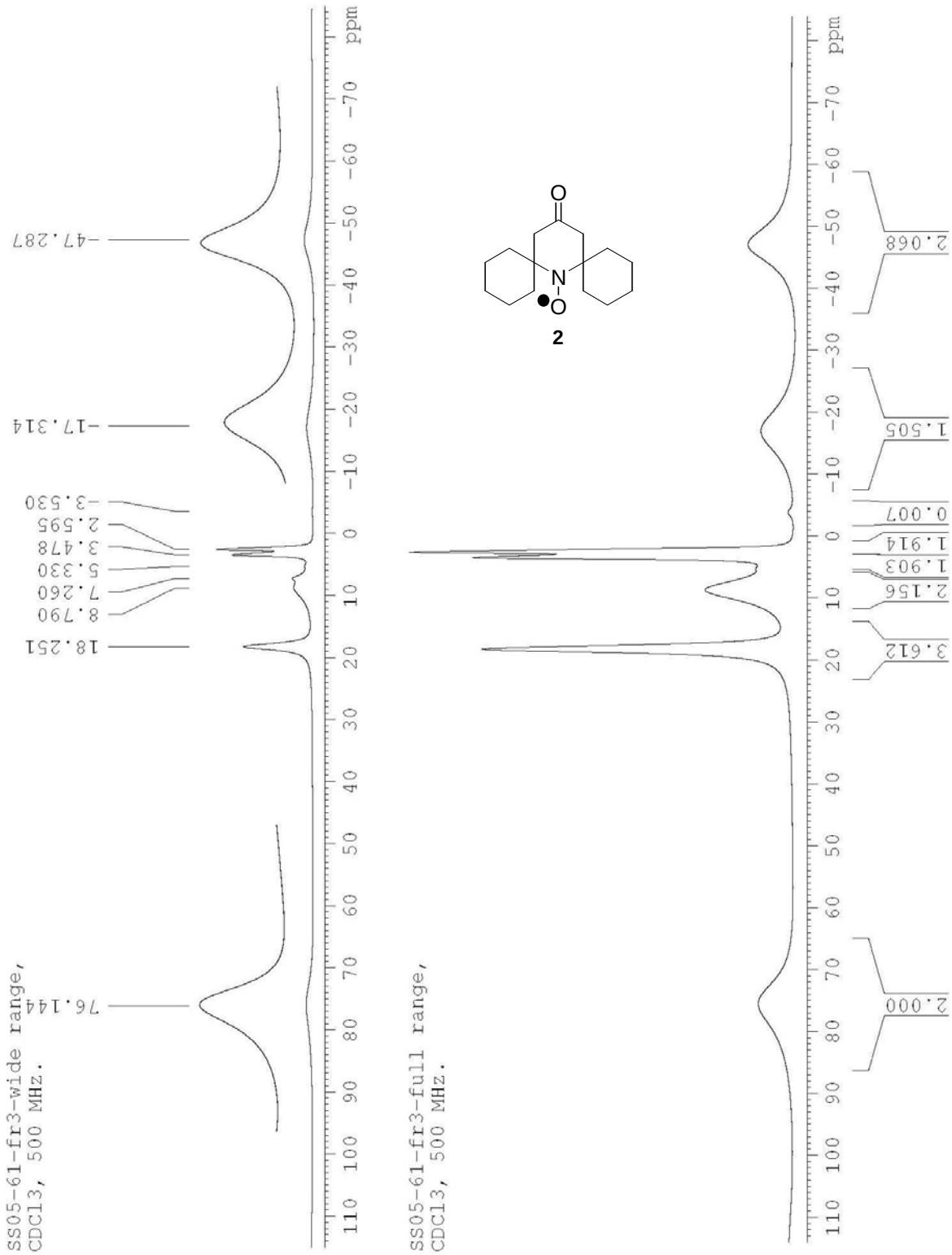

Figure S12. ^{1}H NMR (500 MHz, chloroform-*d*, LB = 0.30 Hz) spectrum of ketone nitroxide **2** (sample label: SS05-61-fr3). Bottom plot: 104.1 mg in 0.155 mL of chloroform-*d* (2.68 M, SS05-61-fr3-full range). Top plot: after dilution with chloroform-*h* (2.44 M, SS05-61-fr3-wide range).

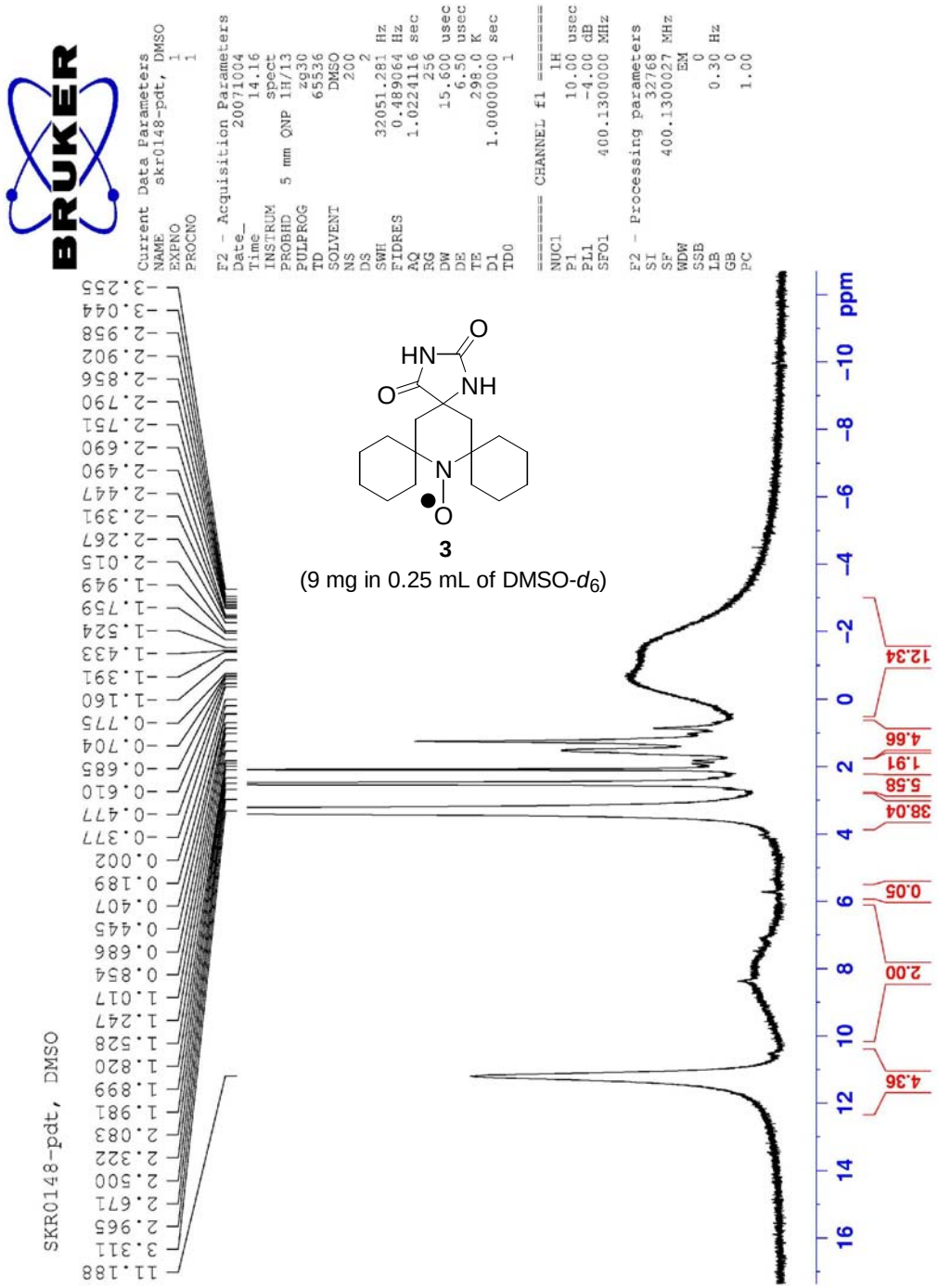

Figure S13. ^{1}H NMR (400 MHz, DMSO-d_6) spectrum of hydantoin nitroxide **3** (SKR0148-pdt).

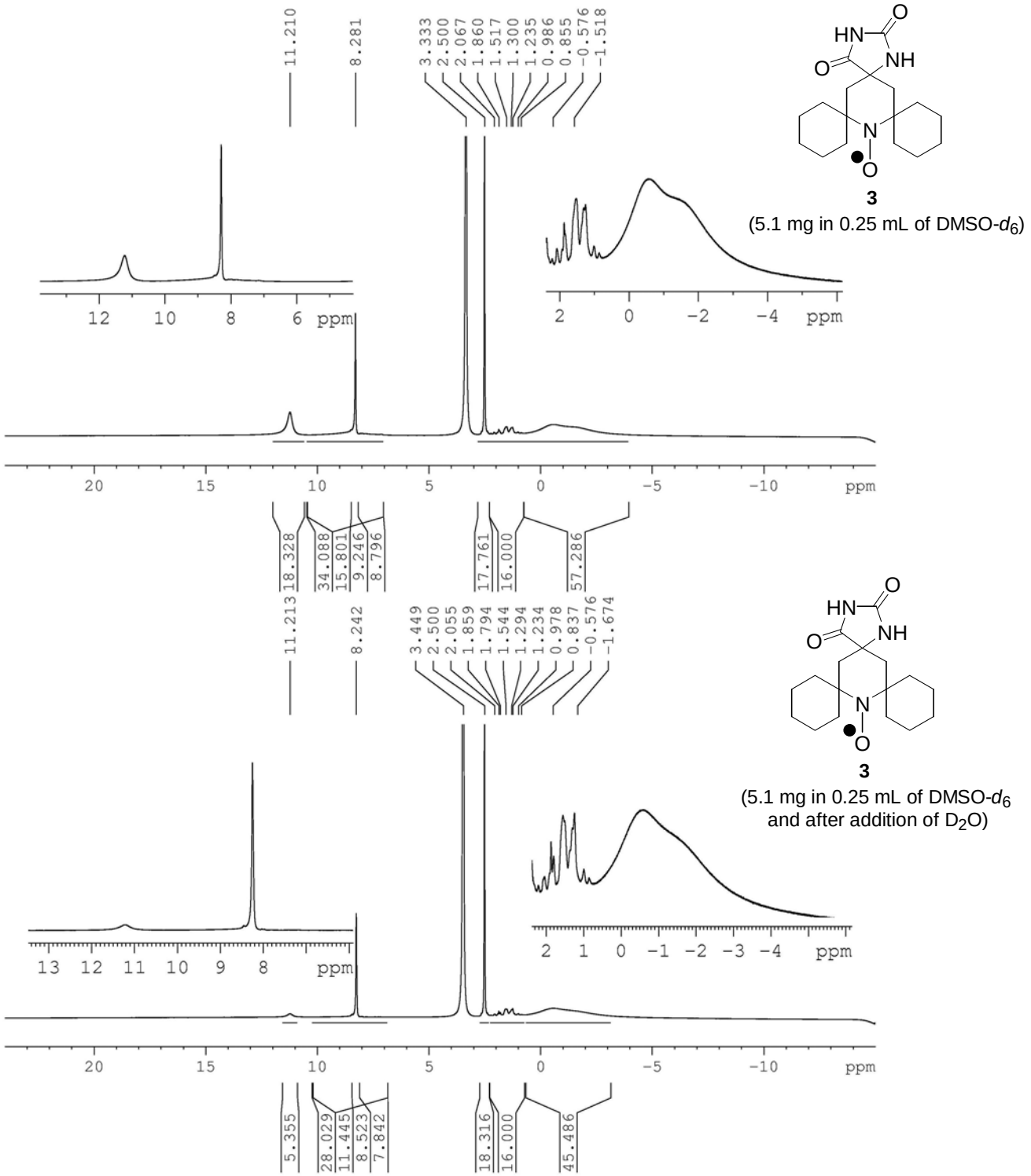

Figure S14. ^{1}H NMR (500 MHz, DMSO-d_6) spectrum and D_2O exchange experiment for hydantoin nitroxide **3** (xsz-3-71-crd1). Top and bottom spectra are taken before and after addition of D_2O. Sharp singlet at about 8 ppm corresponds to residual solvent (chloroform) present in this sample.

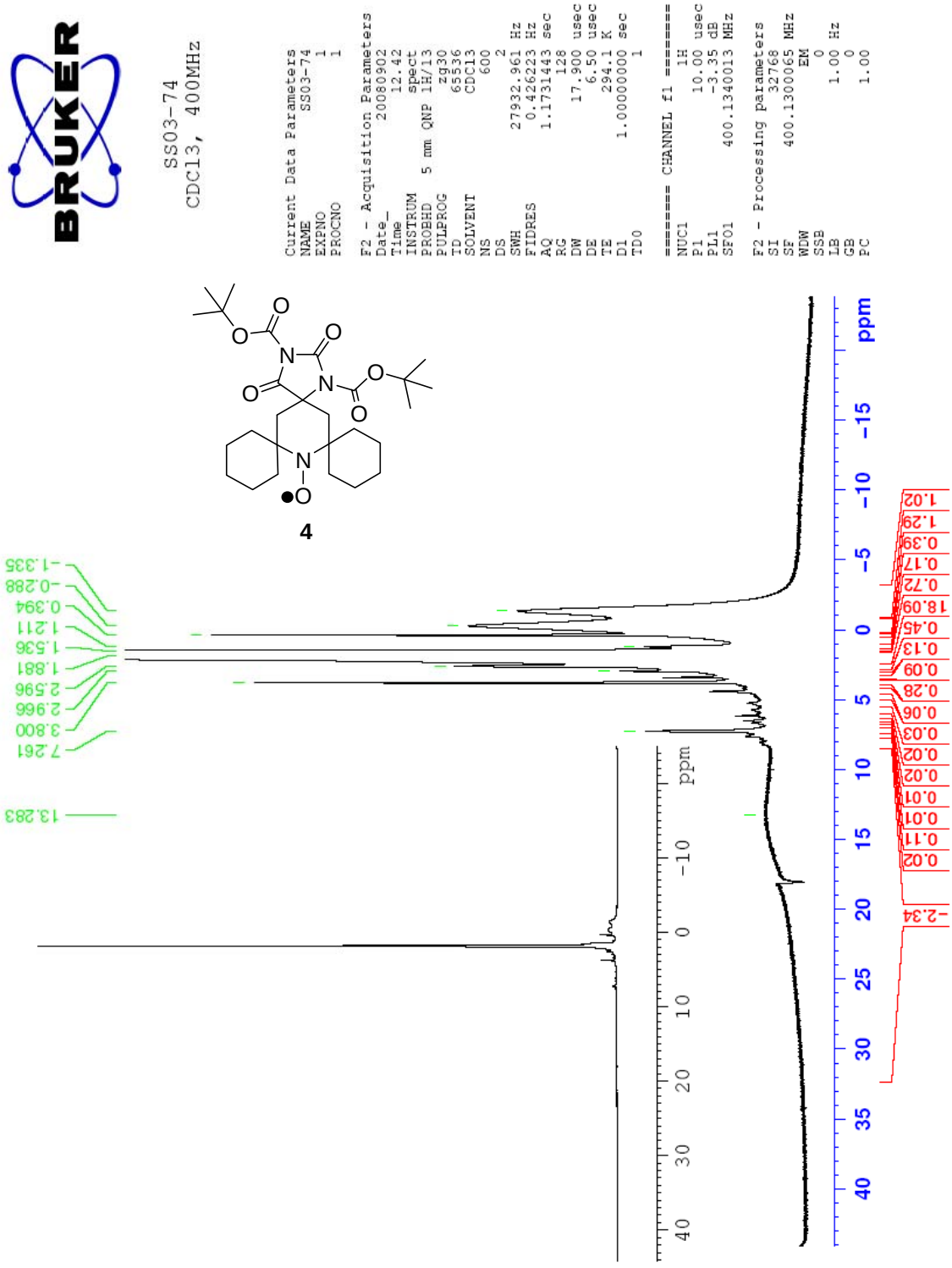

Figure S15. ^{1}H NMR (400 MHz, chloroform-*d*) spectrum of 0.18 M di-Boc-hydantoin nitroxide **4** (ss03-74); solution of nitroxide (19.1 mg) in chloroform-*d* (0.2 mL) in 3-mm tube.

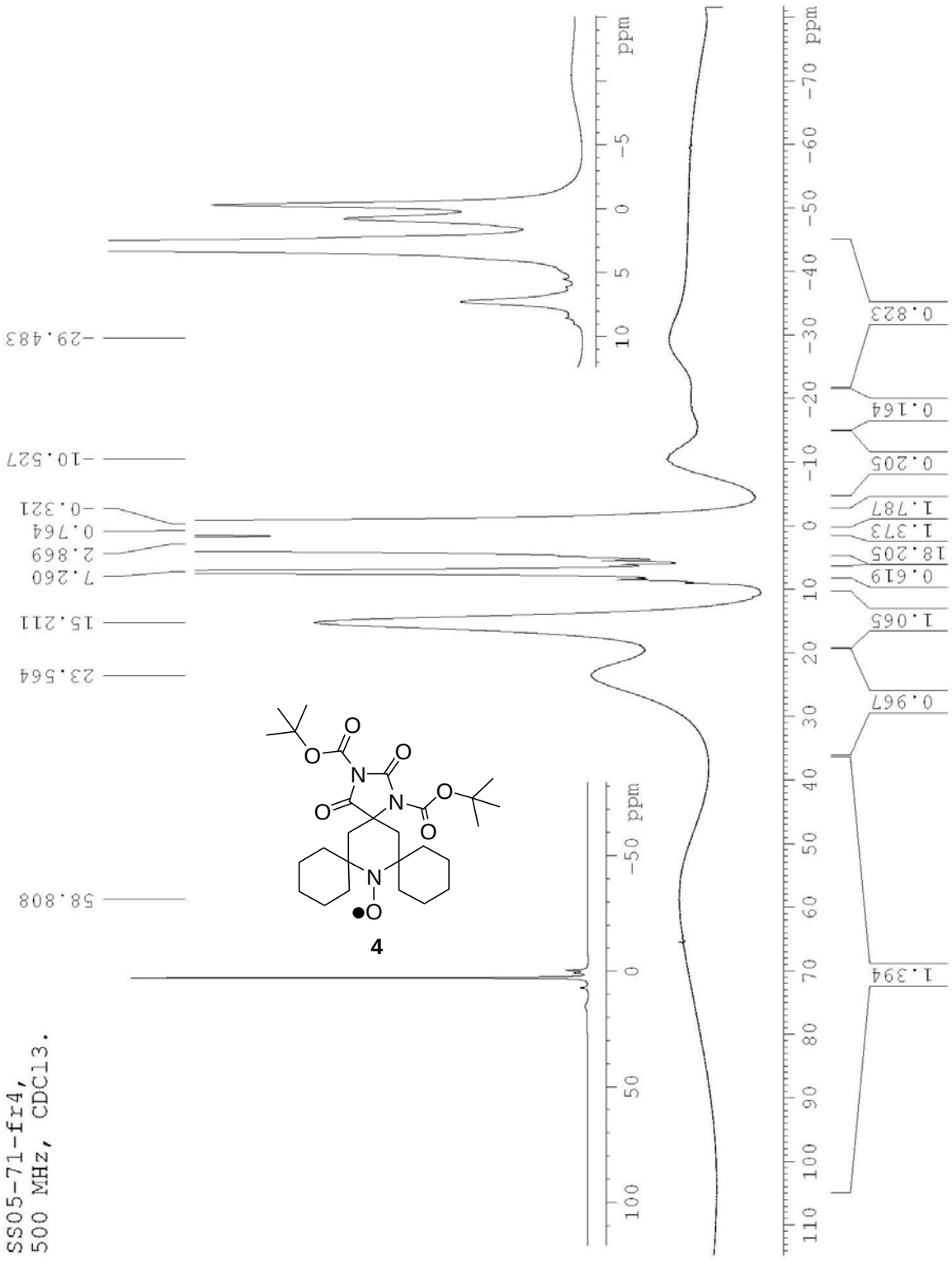

Figure S16. ^{1}H NMR (500 MHz, chloroform-*d*, LB = 4.0 Hz) spectrum of 0.73 M di-Boc hydantoin nitroxide **4** (SS05-71-fr4); solution of nitroxide (55.4 mg) in chloroform-*d* (0.146 mL) in 3-mm tube.

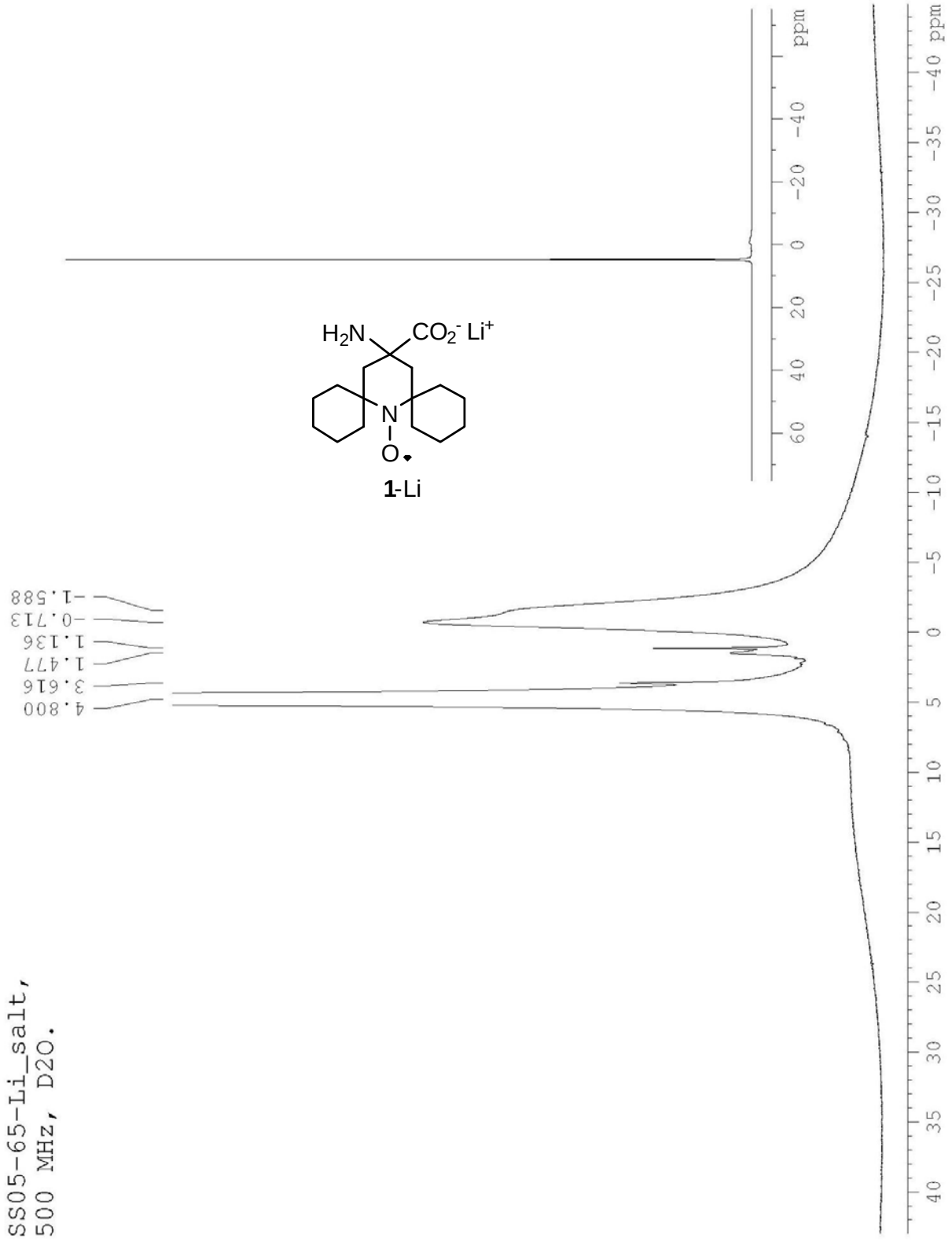

Figure S17. ^{1}H NMR (500 MHz, cryoprobe, D_2O, 0.18 M, SS05-65-Li_salt, LB = 4.0 Hz) spectrum of lithium salt of amino acid nitroxide **1-Li** (5.7 mg zwitterionic amino acid, SS05-65-am ac, in 0.11 mL of 0.44 M LiOD in D_2O).

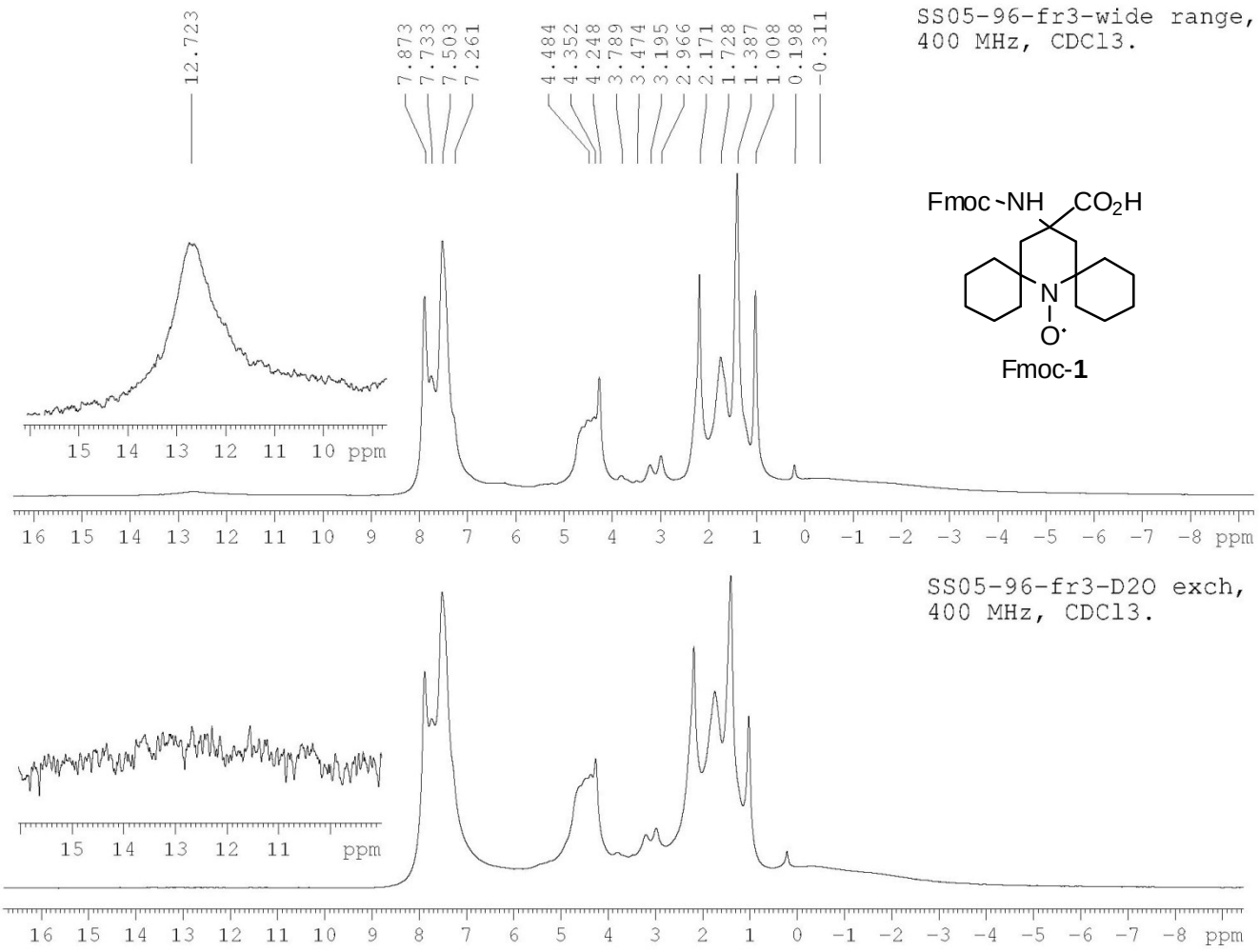

Figure S18. ^{1}H NMR (400 MHz, chloroform-*d*, LB = 12.0 Hz, SS05-96-fr3) spectra and D_2O exchange experiment for Fmoc-amino acid nitroxide **1**. Top spectrum: before addition of D_2O, 0.12 M, 10.3 mg Fmoc-**1** in 0.166 mL of chloroform-*d*. Bottom spectrum: after addition of D_2O.

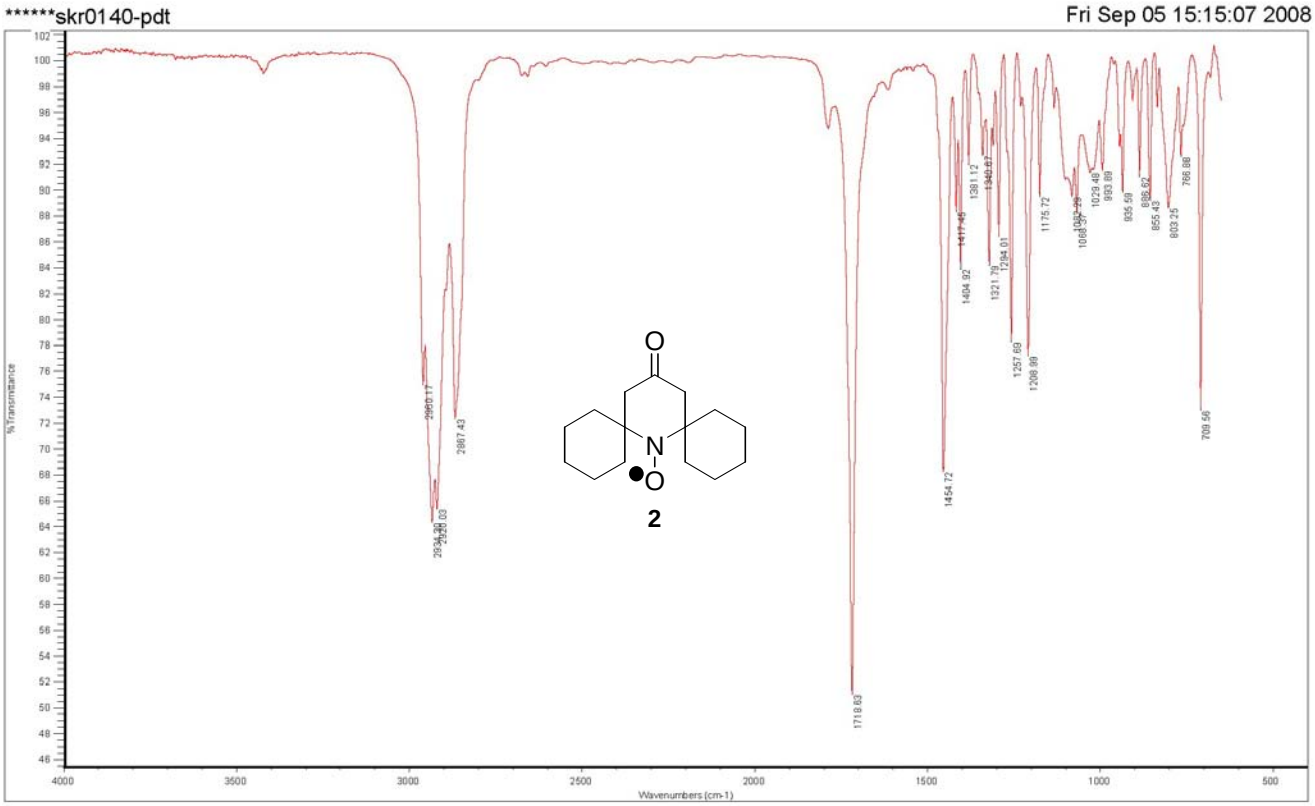

Number of sample scans: 512
Number of background scans: 512
Resolution: 4.000
Sample gain: 1.0
Mirror velocity: 0.6329
Aperture: 100.00

Figure S19. IR (ZnSe, cm^{-1}) spectrum of ketone nitroxide **2** (SKR0140-pdt).

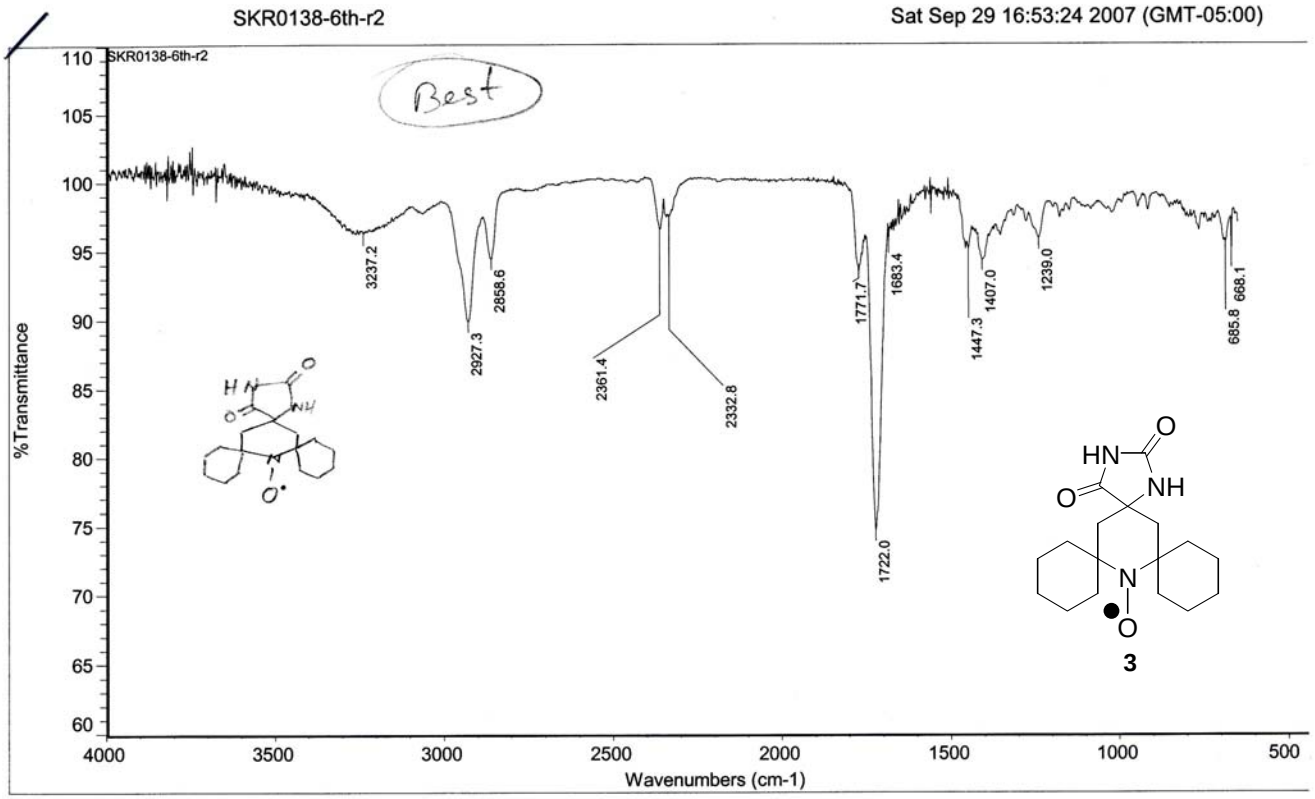

Number of sample scans: 128
Number of background scans: 32
Resolution: 2.000
Sample gain: 4.0
Mirror velocity: 0.6329
Aperture: 100.00

Figure S20. IR (ZnSe, cm^{-1}) spectrum of hydantoin nitroxide **3** (SKR0138-6^{th}-r2).

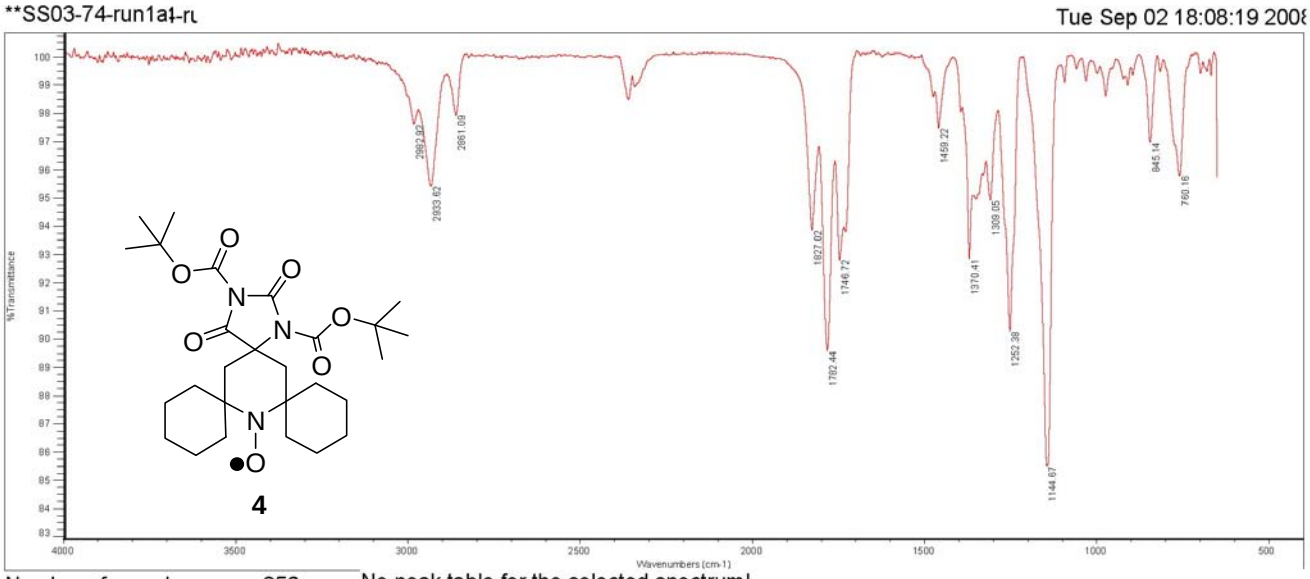

Number of sample scans: 256
Number of background scans: 25
Resolution: 4.000
Sample gain: 1.0
Mirror velocity: 0.6329
Aperture: 100.00

Detector: DTGS KBr
Beamsplitter: KBr
Source: IR

No peak table for the selected spectrum!

Figure S21. IR (ZnSe, cm^{-1}, 256 background scans) spectrum of di-Boc-hydantoin nitroxide **4** (ss03-74-run1a).

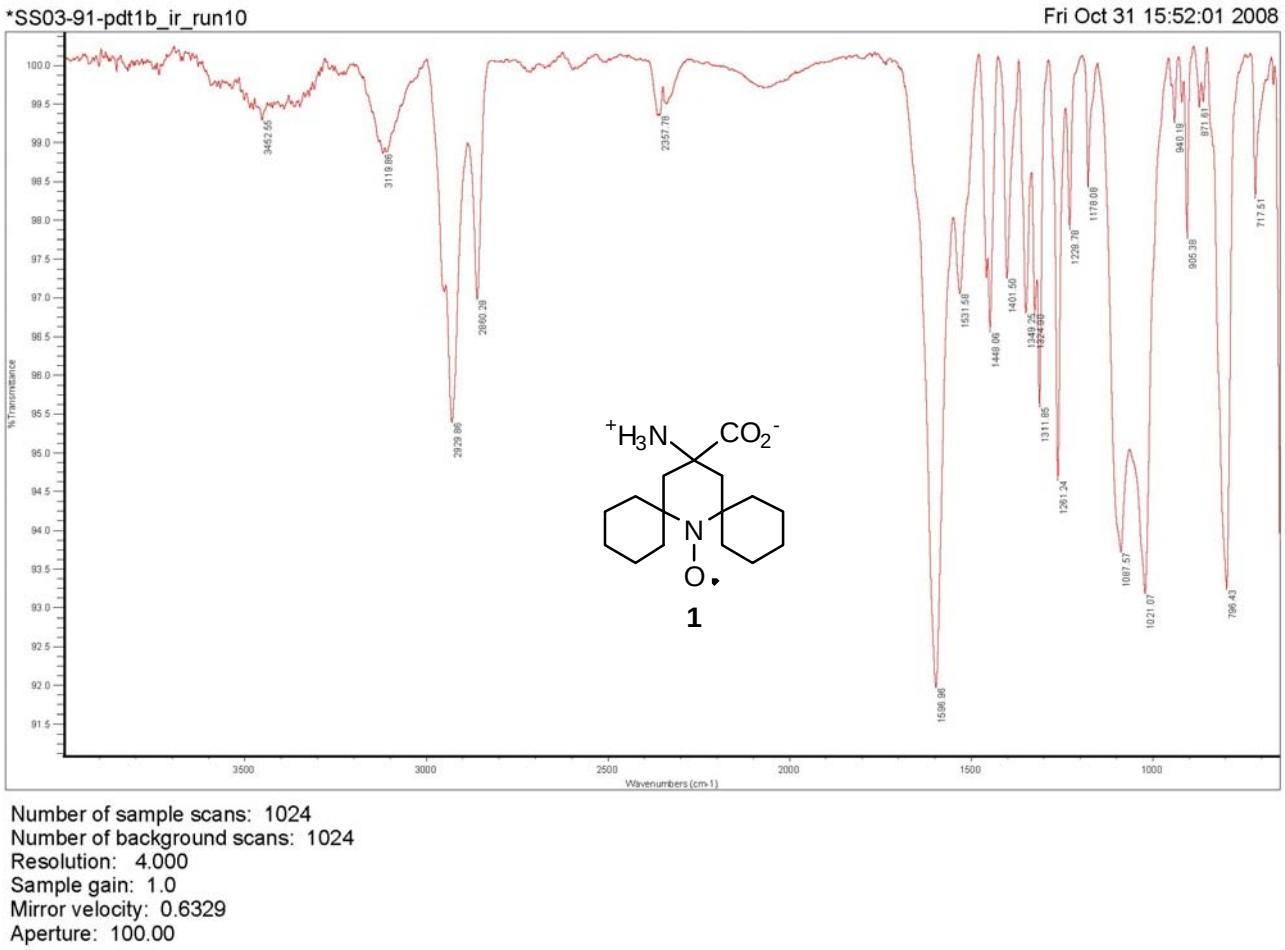

Number of sample scans: 1024
Number of background scans: 1024
Resolution: 4.000
Sample gain: 1.0
Mirror velocity: 0.6329
Aperture: 100.00

Figure S22. IR (ZnSe, cm^{-1}) spectrum of zwitterion amino acid nitroxide **1** (ss03-91-pdt1b). Assignments: 3452 (O-H stretch of the adsorbed water participating in hydrogen bonding), 3120 (N-H stretch of the $-NH_3^+$), 1597 (stretch of the $-COO^-$).

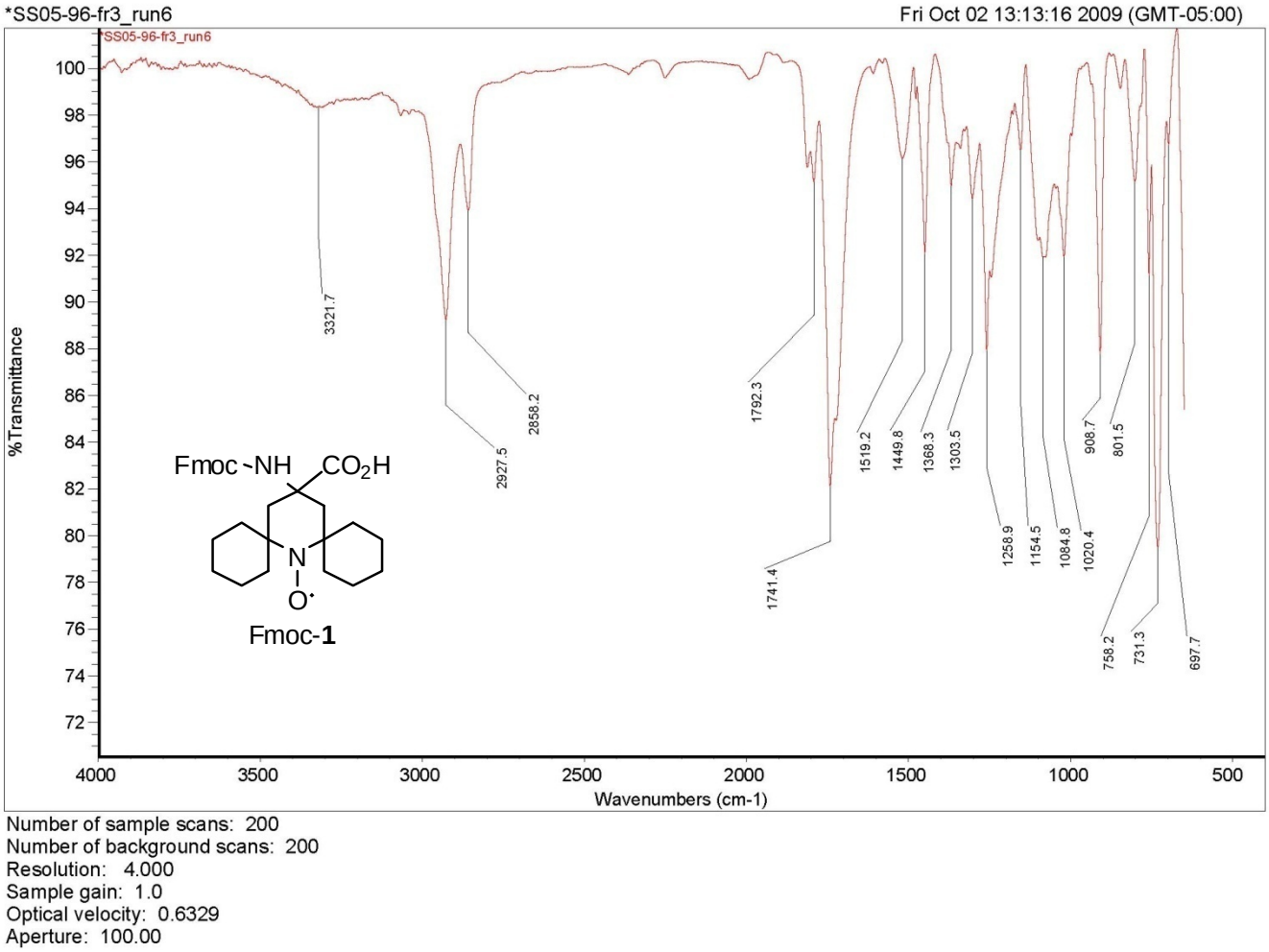

Figure S23. IR (ZnSe, cm^{-1}) spectrum of Fmoc-amino acid nitroxide Fmoc-**1** (SS05-96-fr3).

5. Computational details.

All calculations were performed at 298 K by the Gaussian03 program package running on an 8-cpu workstation under Linux operating system.[25] Ground-state geometries were fully optimized with no symmetry constraints (C_1 point group), starting from the X-ray determined structures for polymorph A, using the B3LYP/6-311+G(d,p) method. The optimized structures were found to be minima by vibrational analyses. For zero-point energies, scaling factor of 0.9877 for the B3LYP/6-311+G(d,p) method was used.[26] The results of calculations are summarized in Table S8.

Table S8. B3LYP/6-311+G(d,p) geometry optimizations and vibrational frequency calculations for hydantoin nitroxide **3**.

	Molecule A Twist-boat geometry		Molecule B Chair geometry	
	X-ray determined	Optimized	X-ray determined	Optimized
Total energy[a]	-1053.44573072	-1053.67775911	-1053.44634513	-1053.67976948
RMS gradient norm[b]	-	8.09×10^{-6}	-	1.63×10^{-6}
Zero-point-energy[c]	-	263.21	-	263.60
Relative energy[c,d]	0.39	0.87	0	0
Vibrational frequencies[e]	-	20.9, 32.9, 68.2	-	18.9, 34.4, 75.0

[a] In Hartrees; 1 Hartree = 627.51 kcal mol^{-1}. [b] In a.u., Cartesian coordinates. [c] In kcal mol^{-1}, scaled ZPE for optimized geometries. [d] Relative energy with respect to the chair. [e] Three lowest frequencies in cm^{-1}.

Optimized Geometry for the Twist-Boat (Molecule A).

```
Stoichiometry    C17H26N3O3(2)
 Framework group  C1[X(C17H26N3O3)]
 Deg. of freedom   141
 Full point group                 C1
 Largest Abelian subgroup         C1      NOp   1
 Largest concise Abelian subgroup C1      NOp   1
                         Standard orientation:
 ---------------------------------------------------------------------
 Center     Atomic     Atomic              Coordinates (Angstroms)
 Number     Number      Type              X           Y           Z
 ---------------------------------------------------------------------
    1          8             0       -1.089588    2.047244    2.037921
    2          8             0        1.131474    4.419962   -1.205501
    3          8             0       -0.153617   -2.970225   -0.399652
    4          7             0       -0.077393    3.520940    0.576408
    5          7             0        0.867084    2.136043   -0.859129
    6          7             0       -0.100973   -1.709261   -0.196665
    7          6             0        4.213083   -1.617878    0.013059
    8          6             0        3.438623   -1.683134    1.335778
    9          6             0        1.966427   -2.058970    1.111273
   10          6             0       -2.280162   -1.567395   -1.343596
   11          6             0       -3.700897   -0.985203   -1.378497
   12          6             0       -4.380689   -1.086980   -0.007869
   13          6             0       -3.523424   -0.432273    1.080922
   14          6             0       -2.093868   -0.994777    1.105264
   15          6             0        0.121605    1.244913    0.039564
   16          6             0       -0.446992    2.283253    1.041878
   17          6             0        0.705669    3.467395   -0.595912
   18          6             0        1.018009    0.250018    0.800590
   19          6             0        1.238464   -1.114092    0.122525
   20          6             0       -1.374754   -0.914610   -0.269028
   21          6             0       -1.018194    0.515778   -0.728023
   22          6             0        2.057218   -1.047114   -1.194427
   23          6             0        3.531435   -0.670707   -0.982859
   24          1             0        4.263787   -2.622660   -0.424477
   25          1             0        5.245299   -1.300464    0.190957
   26          1             0        3.518874   -0.720770    1.855548
   27          1             0        3.893191   -2.422872    2.002079
   28          1             0        1.421886   -2.071369    2.060797
   29          1             0        1.905672   -3.068530    0.701268
   30          1             0       -1.799427   -1.477216   -2.323292
   31          1             0       -2.331389   -2.634335   -1.122665
   32          1             0       -3.686029    0.062067   -1.704728
   33          1             0       -4.282387   -1.526068   -2.131776
   34          1             0       -4.533922   -2.145224    0.238689
   35          1             0       -5.372983   -0.625662   -0.039426
   36          1             0       -3.976509   -0.583065    2.065777
   37          1             0       -3.494623    0.652891    0.930403
   38          1             0       -2.125434   -2.055631    1.375853
   39          1             0       -1.518441   -0.477755    1.873805
   40          1             0       -0.317841    4.392704    1.025414
   41          1             0        1.276926    1.846515   -1.732630
   42          1             0        0.556224    0.070695    1.773870
   43          1             0        1.979248    0.727669    0.993789
   44          1             0       -1.917722    1.133080   -0.724190
   45          1             0       -0.703586    0.448828   -1.772833
   46          1             0        1.997536   -2.042002   -1.646834
   47          1             0        1.582852   -0.364336   -1.906967
   48          1             0        4.049563   -0.697462   -1.946864
   49          1             0        3.612741    0.361721   -0.621862
 ---------------------------------------------------------------------
 Rotational constants (GHZ):      0.3017179      0.2557716      0.1698983
 Standard basis: 6-311+G(d,p) (5D, 7F)
 There are   662 symmetry adapted basis functions of A   symmetry.
 Integral buffers will be    131072 words long.
 Raffenetti 2 integral format.
 Two-electron integral symmetry is turned on.
   662 basis functions,  1036 primitive gaussians,   685 cartesian basis functions
    87 alpha electrons       86 beta electrons
```

Optimized Geometry for the Chair (Molecule B).

```
Stoichiometry    C17H26N3O3(2)
Framework group  C1[X(C17H26N3O3)]
Deg. of freedom   141
Full point group                 C1
Largest Abelian subgroup         C1      NOp   1
Largest concise Abelian subgroup C1      NOp   1
                         Standard orientation:
---------------------------------------------------------------------
Center     Atomic     Atomic              Coordinates (Angstroms)
Number     Number      Type              X           Y           Z
---------------------------------------------------------------------
   1          8             0       -0.023018    2.576916    2.531678
   2          8             0       -0.151561    3.973565   -1.842848
   3          8             0        0.059985   -2.900604   -0.067125
   4          7             0       -0.085609    3.604044    0.460041
   5          7             0       -0.029145    1.857242   -0.890505
   6          7             0        0.037692   -1.659594    0.246365
   7          6             0        4.261391   -1.324334   -0.601501
   8          6             0        3.306246   -0.500687   -1.473964
   9          6             0        1.847226   -0.949735   -1.303033
  10          6             0       -1.805572   -1.021525   -1.294414
  11          6             0       -3.279477   -0.620832   -1.458135
  12          6             0       -4.201331   -1.476421   -0.580437
  13          6             0       -3.749886   -1.452340    0.885415
  14          6             0       -2.280166   -1.872479    1.024939
  15          6             0       -0.015696    1.258700    0.447049
  16          6             0       -0.039798    2.538861    1.324390
  17          6             0       -0.096284    3.221343   -0.898068
  18          6             0        1.251317    0.460631    0.790408
  19          6             0        1.364633   -0.948963    0.175452
  20          6             0       -1.314770   -0.999872    0.181301
  21          6             0       -1.250609    0.412970    0.796870
  22          6             0        2.364780   -1.785822    1.014636
  23          6             0        3.817821   -1.314038    0.866837
  24          1             0        4.278225   -2.359685   -0.964287
  25          1             0        5.282830   -0.942304   -0.694952
  26          1             0        3.582119   -0.592279   -2.529354
  27          1             0        3.408654    0.562888   -1.228220
  28          1             0        1.738055   -1.976722   -1.663147
  29          1             0        1.196411   -0.332270   -1.926952
  30          1             0       -1.176824   -0.389619   -1.927117
  31          1             0       -1.665463   -2.046089   -1.650651
  32          1             0       -3.416462    0.438621   -1.211690
  33          1             0       -3.557968   -0.721934   -2.511956
  34          1             0       -4.185683   -2.511369   -0.944324
  35          1             0       -5.235462   -1.128667   -0.667660
  36          1             0       -4.368998   -2.129192    1.482285
  37          1             0       -3.907401   -0.450840    1.303633
  38          1             0       -2.163501   -2.905294    0.691073
  39          1             0       -1.964855   -1.838425    2.072476
  40          1             0       -0.113841    4.571525    0.747373
  41          1             0       -0.084872    1.351093   -1.757283
  42          1             0        1.259421    0.367785    1.880047
  43          1             0        2.131680    1.045343    0.518499
  44          1             0       -2.154630    0.965058    0.533839
  45          1             0       -1.247410    0.317632    1.886364
  46          1             0        2.054119   -1.761556    2.063865
  47          1             0        2.283313   -2.822641    0.682648
  48          1             0        3.942071   -0.306926    1.282901
  49          1             0        4.463701   -1.967744    1.461184
---------------------------------------------------------------------
Rotational constants (GHZ):      0.2938472      0.2526769      0.1760830
Standard basis: 6-311+G(d,p) (5D, 7F)
There are   662 symmetry adapted basis functions of A   symmetry.
Integral buffers will be    131072 words long.
Raffenetti 2 integral format.
Two-electron integral symmetry is turned on.
  662 basis functions,  1036 primitive gaussians,   685 cartesian basis functions
   87 alpha electrons       86 beta electrons
```

6. References for supporting information.

1. H. Sato, S. E. Bottle, J. P. Blinco, A. S. Micallef, S. S. Eaton, G. R. Eaton, Electron spin-lattice relaxation of nitroxyl radicals in temperature ranges that span glassy solutions to low-viscosity liquids. *J. Magn. Reson.* **2008**, *191*, 66 - 77.
2. R. W. Quine, S. S. Eaton, G. R. Eaton, Saturation recovery electron paramagnetic resonance spectrometer. *Rev. Sci. Instrum.* **1992**, *63*, 4251-4262.
3. R. W. Quine, G. R. Eaton, S. S. Eaton, Pulsed EPR spectrometer. *Rev. Sci. Instrum.* **1987**, *58*, 1709-1723.
4. K. M. Salikhov, Y. D. Tsvetkov, Electron spin-echo studies of interactions in solids, in *Time Domain Electron Spin Resonance*. (eds. L. Kevan & R.N. Schwartz) 232-277 (Wiley, New York; 1979).
5. A. Zecevic, G. R. Eaton, S. S. Eaton, M. Lindgren, Dephasing of electron spin echoes for nitroxyl radicals in glassy solvents by non-methyl and methyl protons. *Mol. Phys.* **1998**, *95*, 1255-1263.
6. D. E. Budil, K. A. Earle, W. B. Lynch, J. H. Freed, Electron paramagnetic resonance at 1 millimeter wavelength, in *Advanced EPR: Applications in Biology and Biochemistry*. (ed. A.J. Hoff) 307-340 (Elsevier, Amsterdam; 1989).
7. V. Kathirvelu, C. Smith, C. Parks, M. A. Mannan, Y. Miura, K. Takeshita, S. S. Eaton, G. R. Eaton, Relaxation Rates for Spirocyclohexyl Nitroxyl Radicals are Suitable for Interspin Distance Measurements at Temperatures up to about 125 K. *Chem. Commun.* **2009**, 454-456.
8. G. Jeschke, Y. Polyhach, Distance measurements on spin-labeled biomacromolecules by pulsed electron paramagnetic resonance. *Physical Chemistry Chemical Physics* **2007**, *9*, 1895-1910.
9. H. Sato, *et al.* Impact of molecular size on electron spin relaxation rates of nitroxyl radicals in glassy solvents between 100 and 300 K. *Mol. Phys.* **2007**, *105*, 2137-2151.
10. J. Murphy, Spin-lattice relaxation due to local vibrations with temperature-independent amplitudes. *Phys. Rev.* **1996**, *145*, 241-247.
11. J. G. Castle, Jr., D. W. Feldman, Resonance modes at defects in crystalline quartz. *Phys. Rev. A* **1965**, *137*, 671-673.
12. B. H. Robinson, C. Mailer, A. W. Reese, Linewidth analysis of spin labels in liquids. I. Theory and data analysis. *J. Magn. Reson.* **1999**, *138*, 199-209.
13. C. Mailer, R. D. Nielsen, B. H. Robinson, Explanation of Spin-Lattice Relaxation Rates of Spin Labels Obtained with Multifrequency Saturation Recovery EPR. *J. Phys. Chem. A* **2005**, *109*, 4049-4061.
14. R. Owenius, G. E. Terry, M. J. Williams, S. S. Eaton, G. R. Eaton, Frequency Dependence of Electron Spin Relaxation of Nitroxyl Radicals in Fluid Solution. *J. Phys. Chem. B* **2004**, *108*, 9475-9481.
15. P. W. Atkins, D. Kivelson, ESR Linewidths in Solution. II. Analysis of Spin-Rotational Relaxation Data. *J. Chem. Phys.* **1966**, *44*, 169-174.

16. K. Nakagawa, M. B. Candelaria, W. W. C. Chik, S. S. Eaton, G. R. Eaton, Electron-spin relaxation times of chromium(V). *J. Magn. Reson.* **1992**, *98*, 81-91.
17. S. A. Dzuba, Libration motion of guest spin probe molecules in organic glasses: CW EPR and electron spin echo study. *Spectrochim. Acta A* **2000**, *56*, 227-234.
18. H. Sato, V. Kathirvelu, G. Spagnol, S. Rajca, A. Rajca, S. S. Eaton, G. R. Eaton, Impact of electron-electron spin interaction on electron spin relaxation of nitroxide diradicals and tetraradical in glassy solvents between 10 and 300 K. *J. Phys. Chem. B.* **2008**, *112*, 2818-2828.
19. J.-L. Du, G. R. Eaton, S. S. Eaton, Temperature, orientation, and solvent dependence of electron spin-lattice relaxation rates for nitroxyl radicals in glassy solvents and doped solids. *J. Magn. Reson. A* **1995**, *115*, 213-221.
20. SADABS: R. Blessing, *Acta Cryst. A* **1995**, *51*, 33–38.
21. SAINT 6.1, Bruker Analytical X-Ray Systems, Madison, WI, 1999.
22. Sir2004, A Program for Automatic Solution and Refinement of Crystal Structure, M. C. Burla, R. Caliandro, M. Carnalli, B. Carrozzini, G. L. Cascarano, L. De Caro, C. Giacovazzo, G. Polidori, R. Sagna, Version 1.0, 2004.
23. SHELXL-97: SHELXTL-Plus V5.10, Bruker Analytical X-Ray Systems, Madison, WI.
24. Preparation of ketone nitroxide **2** (via the hydrogen peroxide – tungstate oxidation) and its melting point: Y. Miura, N. Nakamura, I. Taniguchi, Low-Temperature "Living" Radical Polymerization of Styrene in the Presence of Nitroxides with Spiro Structures. *Macromolecules* **2001**, *34*, 447–455.
25. M. J. Frisch, G. W. Trucks, H. B. Schlegel, G. E. Scuseria, M. A. Robb, J. R. Cheeseman, J. A. Montgomery Jr., T. Vreven, K. N. Kudin, J. C. Burant, J. M. Millam, S. S. Iyengar, J. Tomasi, V. Barone, B. Mennucci, M. Cossi, G. Scalmani, N. Rega, G. A. Petersson, H. Nakatsuji, M. Hada, M. Ehara, K. Toyota, R. Fukuda, J. Hasegawa, M. Ishida, T. Nakajima, Y. Honda, O. Kitao, H. Nakai, M. Klene, X. Li, J. E. Knox, H. P. Hratchian, J. B. Cross, C. Adamo, J. Jaramillo, R. Gomperts, R. E. Stratmann, O. Yazyev, A. J. Austin, R. Cammi, C. Pomelli, J. W. Ochterski, P. Y. Ayala, K. Morokuma, G. A. Voth, P. Salvador, J. J. Dannenberg, V. G. Zakrzewski, S. Dapprich, A. D. Daniels, M. C. Strain, O. Farkas, D. K. Malick, A. D. Rabuck, K. Raghavachari, J. B. Foresman, J. V. Ortiz, Q. Cui, A. G. Baboul, S. Clifford, J. Cioslowski, B. B. Stefanov, G. Liu, A. Liashenko, P. Piskorz, I. Komaromi, R. L. Martin, D. J. Fox, T. Keith, M. A. Al-Laham, C. Y. Peng, A. Nanayakkara, M. Challacombe, P. M. W. Gill, B. Johnson, W. Chen, M. W. Wong, C. Gonzalez, J. A. Pople, *Gaussian 03*, Revision E.01 (Gaussian, Wallingford, CT, 2004).
26. M. P. Andersson, P. Uvdal, New Scale Factors for Harmonic Vibrational Frequencies Using the B3LYP Density Functional Method with the Triple-ζ Basis Set 6-311+G(d,p). *J. Phys. Chem. A* **2005**, *109*, 2937–2941.